Journal of Statistical Physics, Vol. 113, Nos. 5/6, December 2003 (© 2003)

Determining Modes for Continuous Data Assimilation in 2D Turbulence

Eric Olson[1,2] **and Edriss S. Titi**[1,3,4]

Received August 28, 2002; accepted April 30, 2003

We study the number of determining modes necessary for continuous data assimilation in the two-dimensional incompressible Navier–Stokes equations. Our focus is on how the spatial structure of the body forcing affects the rate of continuous data assimilation and the number of determining modes. We treat this problem analytically by proving a convergence result depending on the H^{-1} norm of f and computationally by considering a family of forcing functions with identical Grashof numbers that are supported on different annuli in Fourier space. The rate of continuous data assimilation and the number of determining modes is shown to depend strongly on the length scales present in the forcing.

KEY WORDS: Determining modes; continuous data assimilation.

1. INTRODUCTION

In the late 1960s satellite-borne observation systems began producing data on the climate that was nearly continuous in time. Charney, Halem, and Jastrow proposed in ref. 5 that the equations of the atmosphere themselves be used to process this data and obtain improved estimates of the current atmospheric state. Their method, called *continuous data assimilation*, is to insert the observational measurements directly into a model as the latter is

Dedicated to the memory of Oscar P. Manley.

[1] Department of Mathematics, University of California, Irvine, California 92697.

[2] Department of Mathematics, University of Nevada, Reno, Nevada 89557; e-mail: ejolson @unr.edu

[3] Mechanical and Aerospace Engineering, University of California, Irvine, California 92697.

[4] Department of Computer Science and Applied Mathematics, Weizmann Institute of Science, Rehovot 76100, Israel.

0022-4715/03/1200-0799/0

being integrated in time. A summary of the use of continuous data assimilation in practical weather forecasting appears in Daley.[12]

Let $u_1(t)$ represent physical reality at time t. We represent the observational measurements corresponding to $u_1(t)$ at time t by $P_\lambda u_1(t)$, where P_λ is a finite-rank orthogonal projection. Here λ represents a parameter, namely the resolution of the measuring equipment, that will be made precise later. Let $u_2(t)$ be the approximation to $u_1(t)$ obtained from continuous data assimilation of the observational measurements $P_\lambda u_1(\tau)$ over the time interval $\tau \in [0, t]$. We will describe the details of constructing $u_2(t)$ later. Our goal is to find conditions on λ in terms of the other physical parameters of the system which guarantee that $u_2(t)$ will converge to $u_1(t)$ as $t \to \infty$. Note that we assume the idealized situation in which the observational measurements $P_\lambda u_1(t)$ are error free; therefore, there is no need for the additional filtering necessary in applications.

Inspired by the work of Browning *et al.*[2] and motivated by applications involving the full dynamics of the atmosphere, we study continuous data assimilation in the simpler case of a viscous two-dimensional incompressible fluid in a periodic domain. Thus, we take the physical reality $u_1(t)$ to be the exact solution of the two-dimensional incompressible Navier–Stokes equations

$$\frac{\partial u_1}{\partial t} + (u_1 \cdot \nabla)\, u_1 - \nu\, \Delta u_1 + \nabla \pi_1 = f, \qquad \nabla \cdot u_1 = 0 \tag{1.1}$$

with initial conditions $u_1(0) = u_0$ on the L-periodic torus $\Omega = [0, L]^2$. Here u_1 represents the Eulerian velocity field, ν the kinematic viscosity, f a body forcing, and π_1 the physical pressure.

It is clear from (1.1) that if $\int_\Omega u_0 = 0$ and $\int_\Omega f = 0$, then $\int_\Omega u_1(t) = 0$ for all time. Therefore, we consider only solutions with zero mean. It follows that at any time t the velocity field, the body forcing, and the pressure may each be represented by a Fourier series of the form

$$a = \sum_{k \in \mathscr{J}} \hat{a}_k \phi_k, \qquad \text{where} \quad \mathscr{J} = \left\{ \frac{2\pi m}{L} : m \in \mathbf{Z}^2 \setminus \{0\} \right\}, \tag{1.2}$$

$\phi_k(x) = e^{ik \cdot x}$ and $\hat{a}_k = \overline{\hat{a}_{-k}}$. Note that the Fourier coefficients corresponding to the velocity and the forcing are $\mathbf{C}^2$-vector valued such that $k \cdot \hat{a}_k = 0$ whereas the coefficients corresponding to the pressure are scalar. Define the L^2 and H^1 norms

$$|a| = L \left\{ \sum_{k \in \mathscr{J}} |\hat{a}_k|^2 \right\}^{1/2} \qquad \text{and} \qquad \|a\| = L \left\{ \sum_{k \in \mathscr{J}} |k|^2\, |\hat{a}_k|^2 \right\}^{1/2}. \tag{1.3}$$

The Fourier space representation provides a convenient way of describing the orthogonal projections needed for our study. For a such that $|a| < \infty$ we define

$$P_\lambda a = \sum_{|k|^2 \leqslant \lambda} \hat{a}_k \phi_k \qquad \text{and} \qquad Q_\lambda = I - P_\lambda. \tag{1.4}$$

Thus, for the projection $P_\lambda u_1(t)$ given above, the quantity $\lambda^{-1/2}$ represents the smallest length scale of the fluid which can be observed—the resolution of the presumed measuring equipment. Note that λ and the rank N of P_λ are essentially proportional in two dimensions.

In light of the results on determining projections postulated by Foias and Temam in ref. 25 and proven in refs. 6, 7, and 28, similar results to those we shall present here are likely to hold for any family of projections P_λ for which there exists constants C_1 and $\gamma > 0$ not depending on the rank N of P_λ such that $|u - P_\lambda u| \leqslant C_1 N^{-\gamma} \|u\|$ for all u such that $\|u\| < \infty$. See also refs. 8 and 32. Further work along these lines appears in ref. 4 for the physically relevant model consisting of the two-dimensional Navier–Stokes equations on the surface of a rotating sphere.

Let us agree that if we were given u_0 exactly, that is, the detailed reality at time $t = 0$, then we could integrate the Navier–Stokes equations and hence get $u_1(t)$ exactly for any $t > 0$. Therefore, the main difficulty is that we can not obtain u_0 exactly by measurement. However, we can obtain $P_\lambda u_1(t)$ over as large an interval in time as needed. The question becomes, how do we find $u_1(t)$ from $P_\lambda u_1(t)$. In general this is not possible, so alternatively, let us find $u_2(t)$, a good asymptotic approximation of $u_1(t)$.

To motivate finding $u_2(t)$ let us rewrite the Navier–Stokes equations (1.1) as a system of two coupled differential equations. Let $u_i = p_i + q_i$ where $p_i = P_\lambda u_i$ and $q_i = Q_\lambda u_i$ for $i = 1, 2$. Since P_λ and Q_λ project onto eigenfunctions of the Δ operator they commute with it. Similarly P_λ and Q_λ commute with the divergence and the gradient. Thus, projecting (1.1) by P_λ and then by Q_λ gives

$$\begin{cases} \dfrac{\partial p_1}{\partial t} + P_\lambda\{(p_1+q_1)\cdot\nabla(p_1+q_1)\} - \nu\,\Delta p_1 + \nabla P_\lambda \pi_1 = P_\lambda f, & \nabla\cdot p_1 = 0 \\ \dfrac{\partial q_1}{\partial t} + Q_\lambda\{(p_1+q_1)\cdot\nabla(p_1+q_1)\} - \nu\,\Delta q_1 + \nabla Q_\lambda \pi_1 = Q_\lambda f, & \nabla\cdot q_1 = 0. \end{cases}$$

Since $p_1(t)$ is given directly by measurement, we need only integrate the second equation to find $u_1(t)$. However, since we do not know $q_1(0)$

integrating the second equation is impossible. Therefore, we compute an approximation $q_2(t)$ of $q_1(t)$ by integrating

$$\frac{\partial q_2}{\partial t} + Q_\lambda\{(p_1+q_2)\cdot\nabla(p_1+q_2)\} - \nu\,\Delta q_2 + \nabla Q_\lambda \pi_2 = Q_\lambda f, \qquad \nabla\cdot q_2 = 0 \tag{1.5}$$

with initial conditions $q_2(0)=\eta$ where $\eta = Q_\lambda\eta$ represents an initial guess of the high modes $q_1(0)$ of the exact solution. Hence, the problem for us is a problem of initialization, and we solve it by initializing the high frequencies any way we want and then integrating.

In the numerical part of this paper we simply take $\eta = 0$, however, an initial approximation of $q_1(0)$ might be more reasonably obtained by taking $\eta = Q_\lambda\Phi(p_1(0))$ where Φ is an approximate inertial manifold for the two-dimensional Navier–Stokes equations. More information on approximate inertial manifolds and their applications may be found in Debussche and Marion,[13] Devulder and Marion,[14] Dubios *et al.*,[17] Foias *et al.*,[19, 20] and refs. 15, 18, 23, 30, 42, and references therein.

A systematic computational study of continuous data assimilation in decaying two-dimensional turbulence was first performed by Browning *et al.*[2] In ref. 2, computations were done on the 2π-periodic torus with viscosity $\nu = 10^{-5}$, forcing $f = 0$ and $\eta = 0$. First, a highly accurate reference calculation was made to obtain the solution $u_1(t)$ of (1.1) starting from prescribed initial conditions u_0 such that $|u_0| = 1$. The observational measurements $P_\lambda u_1(t)$ were saved and subsequently used for assimilation into a second calculation to obtain $u_2(t)$. Notice that since the forcing is zero, both u_1 and u_2 eventually converge to zero. However, short time transient behavior may be studied, for example, by monitoring the relative error $|u_1(t)-u_2(t)|/|u_1(t)|$. Under these conditions, it was observed in ref. 2 that continuous data assimilation of the 64 lowest Fourier modes of u_1 was sufficient to accurately reconstruct the small scales of u_1, but assimilation of the 16 lowest modes was not. A similar study of decaying three-dimensional turbulence was recently completed by Kreiss and Yström in ref. 33. In this paper we generalize ref. 2 by considering a nonzero body forcing f to avoid the difficulties of u_1 and u_2 decaying to zero.

Continuous data assimilation is essentially the simplest algorithm for constructing an approximate solution u_2 suitable for treatment by the theory of determining modes of Foias and Prodi.[22] In this context it is necessary to view u_2 as a solution to a modified two-dimensional Navier–Stokes equations. This may be done by adding the evolution equations for $p_1(t)$ to the evolution equations for $q_2(t)$. Thus, we obtain

$$\frac{\partial u_2}{\partial t} + (u_2\cdot\nabla)\,u_2 - \nu\,\Delta u_2 + \nabla\pi_2 = f_2, \qquad \nabla\cdot u_2 = 0 \tag{1.6}$$

with initial conditions $u_2(0) = P_\lambda u_0 + \eta$ where $\eta = Q_\lambda \eta$ and

$$f_2 = f + P_\lambda\{(u_2 \cdot \nabla)\, u_2 - (u_1 \cdot \nabla)\, u_1\}. \tag{1.7}$$

Note that f_2 is a complicated time-dependent feedback forcing function that depends on u_2 to ensure that $P_\lambda u_1(t) = P_\lambda u_2(t)$ for all time $t \geqslant 0$.

The theory of determining modes, however, makes no assumptions on how u_2 was obtained. So, for a moment, let us forget that u_2 was constructed by continuous data assimilation and simply suppose it to be another solution to the Navier–Stokes equations with a given time dependent forcing $f_2(t)$. To avoid possible confusion we shall refer to independent solutions of the standard incompressible two-dimensional Navier–Stokes equations (1.1) by v_1 and v_2 and their corresponding forcing functions by g_1 and g_2 when discussing the general theory of determining modes.

Definition 1.1. The *number of determining modes* is the rank of the smallest projection P_λ such that for any two solutions v_1 and v_2 of (1.1) the convergence $|P_\lambda v_1(t) - P_\lambda v_2(t)| \to 0$ as $t \to \infty$ guarantees that $|v_1(t) - v_2(t)| \to 0$ as $t \to \infty$. We denote by λ_c the smallest value of λ such that the rank of P_λ is equal to the number of determining modes N_c.

It was first shown in ref. 22 that the two-dimensional Navier–Stokes equations possess a finite number of determining modes. At about the same time a result more directly related to continuous data assimilation was independently proved by Ladyzhenskaya.[35] It is clear that the number of determining modes should depend on the forcing, the viscosity, and the size of the domain. In ref. 43 Trève and Manley gave a physical argument relating the number of determining modes in Rayleigh–Bénard convection to the Rayleigh number divided by the Prandtl number. By identifying the buoyancy force in Rayleigh–Bénard convection with the body forcing in the Navier–Stokes equations this lead to

Definition 1.2. The *Grashof number* is defined as

$$\mathrm{Gr}(f) = (L/2\pi\nu)^2 \limsup_{t \to \infty} |f(t)|.$$

The first reasonable rigorous estimate on the number of determining modes in terms of the Grashof number was provided by Foias *et al.*[21] It was observed by Foias and Temam in refs. 24 and 31 that the theory of determining modes can be extended to families of Navier–Stokes equations with asymptotically equivalent body forcing. This is of particular interest to us,

since the forcing function f_2 in continuous data assimilation is not equal to f. The best estimate to date in the periodic case is given in ref. 32 which we shall restate here as

Theorem 1.3. Let v_1 and v_2 be two solutions of the two-dimensional Navier–Stokes equations on the L-periodic torus with corresponding forcing functions g_1 and g_2 and possibly different initial conditions. Then there exists a constant c_1 independent of ν, L, g_i, or of any initial conditions such that for every $\lambda(L/2\pi)^2 > c_1 \operatorname{Gr}(g_1)$ the limits

$$|g_1(t)-g_2(t)| \to 0 \quad \text{and} \quad |P_\lambda v_1(t)-P_\lambda v_2(t)| \to 0 \qquad \text{as} \quad t \to \infty$$

imply that

$$\|v_1(t)-v_2(t)\| \to 0 \qquad \text{as} \quad t \to \infty.$$

Before proceeding, let us first note that a minor modification of the proof of Theorem 1.3 presented in ref. 32 allows us to relax the hypothesis on g_1 and g_2. In particular, it is sufficient to require in Theorem 1.3 that $|Q_\lambda g_1(t)-Q_\lambda g_2(t)| \to 0$ as $t \to \infty$. The intuitive reason for this is clear. Since the difference of the low modes of v_1 and v_2 is already controlled by hypothesis and converge to zero, then all we need to show is that the difference of the high modes of v_1 and v_2 converge to zero. Therefore only the difference of the high modes of g_1 and g_2 need enter into the proof. In light of this observation, Theorem 1.3 may be rewritten as

Theorem 1.4. Let v_1 and v_2 be two solutions of the two-dimensional Navier–Stokes equations on the L-periodic torus with corresponding forcing functions g_1 and g_2 and possibly different initial conditions. Then there exists a constant c_1 independent of ν, L, g_i, or of any initial conditions such that for every $\lambda(L/2\pi)^2 > c_1 \operatorname{Gr}(g_1)$ the limits

$$|Q_\lambda g_1(t)-Q_\lambda g_2(t)| \to 0 \quad \text{and} \quad |P_\lambda v_1(t)-P_\lambda v_2(t)| \to 0 \qquad \text{as} \quad t \to \infty$$

imply

$$\|v_1(t)-v_2(t)\| \to 0 \qquad \text{as} \quad t \to \infty.$$

Thus, we may choose the low modes of g_1 and g_2 to be anything we like provided this choice ensures $|P_\lambda v_1(t)-P_\lambda v_2(t)| \to 0$ as $t \to \infty$. In the case of continuous data assimilation we note that $|Q_\lambda g_1(t)-Q_\lambda g_2(t)| = |Q_\lambda f_1(t)-Q_\lambda f_2(t)| = 0$ and $|P_\lambda v_1(t)-P_\lambda v_2(t)| = |P_\lambda u_1(t)-P_\lambda u_2(t)| = 0$ for

all time $t \geqslant 0$. Therefore, given $\lambda > c_1 \operatorname{Gr}(f)$ and provided that the solution $u_2(t)$ to (1.6) exists, it follows that $\|u_1(t) - u_2(t)\| \to 0$ as $t \to \infty$. In particular, continuous data assimilation works for λ large enough.

We begin our study of how the convergence of u_2 to u_1 is affected by the spatial structure and length scales present in the forcing f by considering the time-independent forcing functions

$$\mathscr{G}(R) = \{f: \operatorname{Gr}(f) = R\}.$$

Given $f \in \mathscr{G}(R)$ let u_1 be the corresponding solution of (1.1). Rescale this solution as follows. Set $\tilde{f}(x) = 8f(2x)$, $\tilde{u}_1(x, t) = 2u_1(2x, 4t)$, $\tilde{\pi}_1(x, t) = 4\pi_1(2x, 4t)$, and $\tilde{u}_0(x) = 2u_0(2x)$. Since $\tilde{f}$, $\tilde{u}_1$, $\tilde{\pi}_1$, and $\tilde{u}_0$ are $L/2$-periodic, then they are also L-periodic. Thus, we find that $\tilde{u}_1$ satisfies

$$\frac{d\tilde{u}_1}{dt} + (\tilde{u}_1 \cdot \nabla)\, \tilde{u}_1 - \nu \Delta \tilde{u}_1 + \nabla \tilde{\pi}_1 = \tilde{f}, \qquad \nabla \cdot \tilde{u}_1 = 0 \tag{1.8}$$

with initial conditions $\tilde{u}_1(0) = \tilde{u}_0$ on the L-periodic torus. That is, $\tilde{u}_1$ is a solution to the two-dimensional Navier–Stokes equations with forcing $\tilde{f}$. Since $|\tilde{f}| = 8\,|f|$ then $\tilde{f} \in \mathscr{G}(8R)$. It follows that for every $f \in \mathscr{G}(R)$ there is an $\tilde{f} \in \mathscr{G}(8R)$ such that the corresponding solutions u_1 and $\tilde{u}_1$ have exactly the same dynamics.

Although the $L/2$-periodic solutions of (1.8) comprise only a small portion of all solutions on the L-periodic domain, the above observation indicates that the Grashof number alone cannot determine the dynamical complexity of the two-dimensional Navier–Stokes equations. Therefore, in order to conduct a more detailed analysis we consider the negative Sobolev norm or dual norm of $\|f\|$ defined as

$$\|f\|_* = L \left\{ \sum_{k \in \mathscr{J}} |k|^{-2}\, |\hat{f}_k|^2 \right\}^{1/2}. \tag{1.9}$$

As we shall see below, this norm will be useful in obtaining a determining modes result which distinguishes between forcing functions with the same Grashof number that are supported on different spatial length scales. Namely, we shall prove

Theorem 1.5. Let $u_1(t)$ be a solution on the global attractor of the two-dimensional Navier–Stokes equations (1.1) with time-independent forcing $f \in L^2(\Omega)$. Let $u_2(t)$ be the approximation to $u_1(t)$ obtained from the continuous data assimilation (1.6) of the observational measurements

$P_\lambda u_1(\tau)$ over the time interval $\tau \in [0, t]$. Then there are constants K_1 and K_2 independent of all initial conditions such that

(i) If there exists α such that $0 < 2\alpha \leqslant \nu\lambda - c_1^2 \nu^{-3} \|f\|_*^2$, then

$$|u_1(t) - u_2(t)| \leqslant |u_1(0) - u_2(0)| \, K_1 e^{-\alpha t} \qquad \text{for} \quad t \geqslant 0.$$

(ii) If there exists α such that $0 < 2\alpha \leqslant \nu\lambda - c_1^2 (\nu^3 \lambda)^{-1} |f|^2$, then

$$\|u_1(t) - u_2(t)\| \leqslant \|u_1(0) - u_2(0)\| \, K_2 e^{-\alpha t} \qquad \text{for} \quad t \geqslant 0.$$

Note that Theorem 1.5 shows that the convergence of u_2 to u_1 is, in fact, exponential in time. This leads us to the following definition.

Definition 1.6. The rate of continuous data assimilation of enstrophy is the supremum over all α such that $\|u_1(t) - u_2(t)\| = O(e^{-\alpha t})$ as $t \to \infty$.

This paper consists of analysis followed by computational results. First we place Eqs. (1.1) and (1.6) in the appropriate functional settings that allow rigorous mathematical analysis of their solutions. We then state a number of important inequalities and facts that we shall need later on. The main goal of our work is to demonstrate that there is a strong relationship between the spatial structure of f, the rate of continuous data assimilation, and the number of determining modes in continuous data assimilation.

Our analysis begins by showing the continuous data assimilation equations (1.6) are globally well posed. For computational relevance we restrict our attention to strong solutions. We then establish a number of lemmas and eventually prove Theorem 1.5. We close with a discussion of whether the system of equations given by (1.1) and (1.6) is dissipative. When $\lambda = 0$ this system is dissipative since in this case $f_2 = f$ and the feedback term $P_\lambda\{(u_2 \cdot \nabla) u_2 - (u_1 \cdot \nabla) u_1\} = 0$. Thus u_2 is a solution of the two-dimensional Navier–Stokes equations for forcing f. For

$$\lambda > \min\{c_1^2 \nu^{-4} \|f\|_*^2, \, c_1 \nu^{-2} |f|\} \tag{1.10}$$

dissipativity follows from the convergence of u_2 to u_1 as in Theorem 1.5. However, for intermediate values of λ the dissipativity of the continuous data assimilation equations remains in question.

Our computational results consist of two sets of experiments. All experiments were performed with $\nu = 0.0001$ and $\eta = Q_\lambda u_2(0) = 0$ on the 2π-periodic torus for forcing functions with a Grashof number of $R = 250000$. Guided by Theorem 1.5 we first consider time-independent

forcing functions $f \in \mathcal{G}(R)$ supported on an annulus in Fourier space. Thus, f may be written

$$f = \sum_{\lambda_m \leq |k|^2 \leq \lambda_M} \hat{f}_k \phi_k. \tag{1.11}$$

with $\hat{f}_k = \overline{\hat{f}_{-k}}$, $k \cdot \hat{f}_k = 0$, and $\hat{f}_0 = 0$. We take the width of the annulus to be

$$\lambda_M - \lambda_m = 4\lambda_f^{1/2} - 2 \qquad \text{where} \quad \lambda_f = (\lambda_m + \lambda_M)/2.$$

The width of the annulus is proportional to the wave number about which it is centered. It was shown by Constantin *et al.*[10] that no Kolmogorov flow, that is no flow driven by forcing only one Fourier mode, can sustain a Kraichnan inertial range spectrum in a statistically steady state. However, two eigenmodes may be sufficient. When $\lambda_f \geqslant 1$ our condition ensures that f forces Fourier modes over a range of different eigenvalues. In particular, these forcing functions generate nonlinear interactions leading to time-dependent flows involving all the Fourier modes. This avoids the forcing functions exhibited by Marchioro in ref. 37 which lead to steady flows which are globally asymptotically stable for any Reynolds number. In particular, Marchioro obtains

Theorem 1.7. If f is supported on the collection of all modes in Fourier space corresponding to the lowest eigenvalue, then the solution to (1.1) converges to a steady flow which is globally asymptotically stable.

Constantin, Foias, and Temam give a simplified proof of this result in ref. 11.

For any given λ_f let $\mathcal{F}(\lambda_f)$ be the set of all functions f of the form (1.11) such that $\mathrm{Gr}(f) = R$. In this way we obtain a one parameter family of subsets $\mathcal{F}(\lambda_f)$ of $\mathcal{G}(R)$ such that each subset consists of functions supported only on certain specified spatial length scales. For functions $f \in \mathcal{F}(\lambda_f)$ we have that

$$(\lambda_f^{1/2} + 1)^{-2} |f|^2 \leqslant \|f\|_*^2 \leqslant (\lambda_f^{1/2} - 1)^{-2} |f|^2. \tag{1.12}$$

Therefore, $\|f\|_*$ decreases for $f \in \mathcal{F}(\lambda_f)$ as λ_f increases.

In our first set of experiments we vary λ_f from 25 through 625 and select functions $f \in \mathcal{F}(\lambda_f)$ by choosing the amplitudes of the coefficients $\hat{f}_k$ in (1.11) according to a Gaussian distribution. For each function selected, a number of continuous data assimilation experiments were conducted using different values of λ for the observational measurements

$P_\lambda u_1(t)$. We measure how the rate of continuous data assimilation α depends on the data assimilation parameter λ and the forcing length-scale parameter λ_f. For each forcing function f, the number of determining modes is consequently the rank of the smallest projection P_λ for which α is clearly positive.

The results in the first half of Table I are, at first, rather surprising. The analytical bounds in part (i) of Theorem 1.5 suggest that the number of determining modes should decrease as λ_f increases; however, our computations indicate that the number of determining modes actually increases by more than an order of magnitude while λ_f ranges from 25 to 361. Only for λ_f greater than 361 does the number of determining modes given by our calculations reflect the decrease of $\|f\|_*$ as λ_f increases.

Why does a flow driven by a function in $\mathscr{F}(484)$ require more determining modes than a flow driven by a function in $\mathscr{F}(25)$? We conduct a second set of computational experiments to shed some light on the cause of this phenomenon. Given $f_L \in \mathscr{F}(25)$ and $f_H \in \mathscr{F}(484)$ we set $f = \theta_L f_L + \theta_H f_H$ where $\theta_L^2 + \theta_H^2 = 1$. In this way we obtain forcing functions supported on two disjoint annuli in Fourier space—one on small wave numbers, the other on large. Here θ_L and θ_H are parameters determining the relative weights of the large and small length scales in the forcing. When θ_H is close to zero f may be viewed as the perturbation of the large scales f_L by the small scales f_H; when θ_L is close to zero f is the perturbation of the small scales f_H by the large scales f_L. We determine which perturbation more significantly affects the number of determining modes computationally in Table II.

As shown by the first three columns, perturbing the small scales by the large scales has the greatest effect. This suggests that it is the absence of an increasing number of large length scales in the forcing which is primarily responsible for the increase in number of determining modes as λ_f ranges from 25 though 361 in the first set of experiments.

We dedicate this paper to the memory of Oscar P. Manley, a good friend and source of encouragement, whose interest and physical insight motivated and laid the foundations for our work.

2. PRELIMINARIES

In this section we characterize the spaces H, V, and V' which appear in the study of the Navier–Stokes equations and state a number of inequalities and facts that we shall need later on. For further details, see, for example, Constantin and Foias,[9] Doering and Gibbon,[16] Robinson,[39] or Temam.[40, 41]

First, define the spaces V_α in terms of the formal Fourier series (1.2) as

$$V_\alpha = \left\{ u = \sum_{k \in \mathcal{J}} \hat{u}_k \phi_k : \|u\|_\alpha^2 < \infty,\ \hat{u}_k = \overline{\hat{u}_{-k}},\ k \cdot \hat{u}_k = 0, \text{ and } \hat{u}_0 = 0 \right\}$$

where the norm

$$\|u\|_\alpha^2 = L^2 \sum_{k \in \mathcal{J}} |k|^{2\alpha} |\hat{u}_k|^2. \tag{2.1}$$

Note that

$$\|u\|_\alpha = \sup\{\langle u, v\rangle : v \in V_{-\alpha} \text{ and } \|v\|_{-\alpha} = 1\} \tag{2.2}$$

where the pairing

$$\langle u, v\rangle = L^2 \sum_{k \in \mathcal{J}} \hat{u}_k \cdot \hat{v}_{-k}.$$

Fourier theory implies that V_α is a subspace of $L^2(\Omega)$ for $\alpha \geqslant 0$. Furthermore, $V_{-\alpha}$ may be identified with the continuous dual of V_α.

A relation exists between the norms defined in (2.1) and the projections defined in (1.4) which allows us to bound the norms of $Q_\lambda u$ and $P_\lambda u$ in a way that depends on the resolution parameter λ. For $\alpha < \beta$ we obtain the following version of the Poincaré inequality

$$\|Q_\lambda u\|_\alpha^2 = L^2 \sum_{|k|^2 > \lambda} |k|^{2\alpha} |\hat{u}_k|^2 \leqslant \frac{L^2}{\lambda^{\beta-\alpha}} \sum_{|k|^2 > \lambda} |k|^{2\beta} |\hat{u}_k|^2 = \frac{1}{\lambda^{\beta-\alpha}} \|Q_\lambda u\|_\beta^2, \tag{2.3}$$

and for $\alpha > \beta$ we obtain the inequality

$$\|P_\lambda u\|_\alpha^2 = L^2 \sum_{|k|^2 \leqslant \lambda} |k|^{2\alpha} |\hat{u}_k|^2 \leqslant L^2 \lambda^{\alpha-\beta} \sum_{|k|^2 \leqslant \lambda} |k|^{2\beta} |\hat{u}_k|^2 = \lambda^{\alpha-\beta} \|P_\lambda u\|_\beta^2. \tag{2.4}$$

Since $Q_{\lambda_1} u = u$ for $\lambda_1 = (2\pi/L)^2$ then (2.3) yields the usual Poincaré inequality

$$\|u\|_\alpha^2 \leqslant \frac{1}{\lambda_1^{\beta-\alpha}} \|u\|^2 \qquad \text{for} \quad \alpha < \beta. \tag{2.5}$$

The functional spaces for solving (1.1) and (1.6) may now be defined as $H = V_0$, $V = v_1$, and $V' = V_{-1}$. Note that the norms $\|u\|_0$, $\|u\|_1$, and $\|u\|_{-1}$ are respectively the norms $|u|$, $\|u\|$, and $\|u\|_*$ given in (1.3) and (1.9). Thus, H consists of the square-integrable functions on the L-periodic torus Ω

which are divergence free and have zero mean, V are those functions in H whose first order derivatives are also square integrable, and V' is the dual of V. Moreover, by Parseval's identity the norms on H and V may also be expressed as $|u| = \{\int_\Omega u \cdot u\}^{1/2}$ and $\|u\| = |\nabla u| = |\nabla \times u|$.

Definition 2.1. Define the Leray projector $P_\sigma: L^2 \to H$ to be the L^2 orthogonal projection from L^2 onto H. Further define $A: V \to V'$ and $B: V \times V \to V'$ to be the continuous extensions of the operators given by

$$Au = -P_\sigma \Delta u \qquad \text{and} \qquad B(u, v) = P_\sigma(u \cdot \nabla v)$$

for any suitably smooth function u. Notice that the domain $D(A)$ of A is V_2.

For $u_0 \in V$ and $f \in H$ we write the Navier–Stokes equations (1.1) as the functional equation in H given by

$$\frac{du_1}{dt} + \nu A u_1 + B(u_1, u_1) = f \tag{2.6}$$

with initial conditions $u_1(0) = u_0$. Under these hypotheses equations (2.6) possess unique strong solutions depending continuously on the initial condition u_0. This is stated specifically as

Theorem 2.2. Let $u_0 \in V$ and $f \in L^2_{\text{loc}}((0, \infty); H)$. Then (2.6) has unique strong solutions that satisfy

$$u_1 \in L^\infty((0, T); V) \cap L^2((0, T); D(A)) \qquad \text{and} \qquad \frac{du_1}{dt} \in L^2((0, T); H)$$

for any $T > 0$. Furthermore, this solution is in $C([0, T]; V)$ and depends continuously on the initial data u_0 in the V norm.

A proof of this theorem can be found, for example, in any of the references 9, 16, 39, or 40 and 41 mentioned above. In the next section we prove a similar result for the continuous data assimilation equations (1.6) governing the evolution of $u_2(t)$. Note that the main difficulty there lies in controlling the feedback forcing f_2.

Let us now recall some algebraic properties of the nonlinear term $B(u, v)$ that play an important role in our analysis. These results may be found in any of the references 9, 16, 39, or 40 and 41. For $u, v, w \in V$ we have that

$$\langle B(u, v), w \rangle = -\langle B(u, w), v \rangle \tag{2.7}$$

and consequently

$$\langle B(u, v), v\rangle = 0. \tag{2.8}$$

Furthermore, if $v \in D(A)$ then

$$(B(v, v), Av) = 0 \tag{2.9}$$

and by differentiation of (2.9) we obtain

$$(B(u, v), Av) + (B(v, u), Av) + (B(v, v), Au) = 0 \tag{2.10}$$

for $u, v \in D(A)$. Note that conditions (2.9) and (2.10) are valid only for the two-dimensional Navier–Stokes equations on a periodic domain.

The nonlinear term may be estimated by Hölder's inequality followed by Ladyzhenskaya's inequality.[34] In order to explicitly estimate the constants appearing in our analysis we state Ladyzhenskaya's inequality here as

Lemma 2.3. Given $u \in V$ then

$$\|u\|_{L^4}^2 \leqslant c_1 \, |u| \, \|u\| \tag{2.11}$$

where $c_1 \leqslant 2 + (2\pi)^{-1}$ for the two-dimensional torus Ω.

With this result in hand, if $u, v, w \in V$ then

$$|\langle B(u, v), w\rangle| \leqslant \|u\|_{L^4} \, \|v\| \, \|w\|_{L^4} \leqslant c_1 \, |u|^{1/2} \, \|u\|^{1/2} \, \|v\| \, |w|^{1/2} \, \|w\|^{1/2}, \tag{2.12}$$

and if $u \in V$, $v \in D(A)$, and $w \in H$ then

$$|\langle B(u, v), w\rangle| \leqslant \|u\|_{L^4} \, \|\nabla v\|_{L^4} \, |w| \leqslant c_1 \, |u|^{1/2} \, \|u\|^{1/2} \, \|v\|^{1/2} \, |Av|^{1/2} \, |w|. \tag{2.13}$$

We end this section with some well known bounds on the time averages of $\|u_1\|$ and $|Au_1|$ in terms of u_0 and f which will be used in the next section.

Lemma 2.4. Let $u_1(t)$ be the unique strong solution to (2.6) with time-dependent forcing $f \in L^2_{\text{loc}}((0, \infty); H)$ and initial condition $u_0 \in V$. Then

$$\frac{1}{t} \int_0^t \|u_1(\tau)\|^2 \, d\tau \leqslant \frac{1}{\nu t} \, |u_0|^2 + \frac{1}{\nu^2 t} \int_0^t \|f(\tau)\|_*^2 \, d\tau \tag{2.14}$$

and

$$\frac{1}{t}\int_0^t |Au_1(\tau)|^2\,d\tau \leqslant \frac{1}{\nu t}\|u_0\|^2+\frac{1}{\nu^2 t}\int_0^t |f(\tau)|^2\,d\tau. \tag{2.15}$$

Proof. The proof may be found in any of the references 9, 16, 39, or 40 and 41. For completeness, we shall present formal calculation here that could be made rigorous if so desired.

To derive the first inequality, multiply (2.6) by u_1 and use (2.8) to obtain

$$\frac{1}{2}\frac{d}{dt}|u_1|^2+\nu\|u_1\|^2=(f,u_1)\leqslant\|f\|_*\|u_1\|.$$

Note that since $u_1\in V$ and $f\in H\subseteq V'$ we may view f as an element of V' and estimate (f,u_1) by $\|f\|_*\|u_1\|$. Applying Young's inequality gives

$$\frac{d}{dt}|u_1|^2+\nu\|u_1\|^2\leqslant\frac{1}{\nu}\|f\|_*^2 \tag{2.16}$$

which upon integrating in time yields

$$|u_1(t)|^2+\nu\int_0^t\|u_1(\tau)\|^2\,d\tau\leqslant|u_0|^2+\frac{1}{\nu}\int_0^t\|f(\tau)\|_*^2\,d\tau.$$

After dropping the first term on the left, inequality (2.14) follows.

To derive the second inequality, multiply (2.6) by Au_1 and use (2.9) to obtain

$$\frac{1}{2}\frac{d}{dt}\|u_1\|^2+\nu|Au_1|^2=(f,Au_1).$$

Applying Cauchy–Schwarz and Young's inequalities gives

$$\frac{d}{dt}\|u_1\|^2+\nu|Au_1|^2\leqslant\frac{1}{\nu}|f|^2 \tag{2.17}$$

which upon integrating in time yields

$$\|u_1(t)\|^2+\nu\int_0^t|Au_1(\tau)|^2\,d\tau\leqslant\|u_0\|^2+\frac{1}{\nu}\int_0^t|f(\tau)|^2\,d\tau.$$

After dropping the first term on the left, inequality (2.15) follows. ∎

3. ANALYTICAL RESULTS FOR CONTINUOUS DATA ASSIMILATION

We treat the continuous data assimilation equations (1.6) as a functional differential equation in the same way that the Navier–Stokes equations (1.1) were treated in the previous section to arrive at the coupled system

$$\begin{cases} \dfrac{du_1}{dt} + \nu A u_1 + B(u_1, u_1) = f \\ \dfrac{du_2}{dt} + \nu A u_2 + B(u_2, u_2) = f + P_\lambda (B(u_2, u_2) - B(u_1, u_1)) \end{cases} \tag{3.1}$$

with initial conditions $u_1(0) = u_0$ and $u_2(0) = P_\lambda u_0 + \eta$ where $u_0 \in V$ and $\eta \in Q_\lambda V$.

The solution to Eq. (3.1) may be viewed as two solutions u_1 and u_2 to the Navier–Stokes equations (2.6) with corresponding forcing f_1 and f_2 given by

$$f_1 = f \qquad \text{and} \qquad f_2 = f + P_\lambda (B(u_2, u_2) - B(u_1, u_1)). \tag{3.2}$$

Note that the forcing function f_2 as defined above is actually the projection with respect to P_σ of the function defined by (1.7) in the introduction. Since f_2 is chosen in a complicated way depending on a feedback with u_2, it is not immediately clear that the second equation in (3.1) is globally well posed. This issue is settled by

Theorem 3.1. Let $T > 0$ and $\lambda \geqslant 0$. If $u_0 = u_1(0) \in V$, $\eta = Q_\lambda u_2(0) \in Q_\lambda V$, and $f \in L^2_{\text{loc}}((0, \infty); H)$ then (3.1) viewed as a system of functional equations in H has a unique strong solution that satisfies

$$u_i \in L^\infty((0, T); V) \cap L^2((0, T); D(A)) \qquad \text{and} \qquad \frac{du_i}{dt} \in L^2((0, T); H) \tag{3.3}$$

for $i = 1, 2$. Furthermore, the solutions are in $C([0, T]; V)$ and depend continuously on the initial data u_0 and η in the V norm.

Proof. First we show existence of solutions. For u_1 this result follows from the classical theory of the Navier–Stokes equations given by Theorem 2.2. For u_2 we use the Galerkin method. Let P_n be the nth

Galerkin projector and assume that n is large enough that $P_\lambda H \subseteq P_n H$. The solution u_2^n to the finite-dimensional Galerkin truncation of the second equation in (3.1) satisfies

$$\frac{du_2^n}{dt} + \nu A u_2^n + P_n B(u_2^n, u_2^n) = P_n f + P_\lambda (B(u_2^n, u_2^n) - B(u_1, u_1)). \tag{3.4}$$

Solutions to this ordinary differential equation exist for short times since the nonlinearity is locally Lipshitz. Long time existence follows from the estimates we will provide shortly. Moreover, since these estimates are uniform in n, the compactness theorems of Aubin[1] can be used to extract subsequences as $n \to \infty$ in such a way that u_2^n converges to a solution to (3.1) satisfying (3.3). Further details may be found, for example, in refs. 9, 16, 39, or 40 and 41. As these techniques are well known, we shall content ourselves here with a formal calculation that could be made rigorous if so desired.

In the estimates that follow, we denote the Galerkin solution u_2^n to (3.4) by u_2 for notational simplicity. Since $u_1 \in C([0, T]; V)$ then there exists M_1 large enough that $\|u_1(t)\| \leqslant M_1$ for all t. The low modes $P_\lambda u_2(t)$ are bounded in any norm since all finite dimensional norms are equivalent and $P_\lambda u_2(t) = P_\lambda u_1(t)$. In particular, the Poincaré inequality (2.4) implies that

$$|AP_\lambda u_2(t)| = |AP_\lambda u_1(t)| \leqslant \lambda^{1/2} \|P_\lambda u_1(t)\| \leqslant \lambda^{1/2} \|u_1(t)\| \leqslant \lambda^{1/2} M_1. \tag{3.5}$$

In the case that f is time independent then there are uniform estimates on $|Au_1(t)|$ for u_1 on the attractor, see, for example, refs. 9, 16, 39, or 40 and 41. In this case we could bound $|AP_\lambda u_2(t)|$ independently of λ.

Estimate the high modes $Q_\lambda u_2(t)$ by taking the inner products of (3.4) with $AQ_\lambda u_2$ to obtain

$$\frac{1}{2}\frac{d}{dt}\|Q_\lambda u_2\|^2 + \nu |AQ_\lambda u_2|^2 = (f, AQ_\lambda u_2) - (B(u_2, u_2), AQ_\lambda u_2). \tag{3.6}$$

The first term on the right side may be estimated using Cauchy–Schwarz and Young's inequalities as

$$(f, AQ_\lambda u_2) \leqslant \frac{2}{\nu}|f|^2 + \frac{\nu}{8}|AQ_\lambda u_2|^2.$$

To estimate the second term use (2.9) and the bi-linearity repeatedly to obtain

$$\begin{aligned}-(B(u_2,u_2),AQ_\lambda u_2) &= (B(u_2,u_2),AP_\lambda u_2)\\ &= (B(P_\lambda u_2,u_2),AP_\lambda u_2)+(B(Q_\lambda u_2,u_2),AP_\lambda u_2)\\ &= (B(Q_\lambda u_2,P_\lambda u_2),AP_\lambda u_2)\\ &\quad +(B(P_\lambda u_2,Q_\lambda u_2),AP_\lambda u_2)+(B(Q_\lambda u_2,Q_\lambda u_2),AP_\lambda u_2).\end{aligned}$$

Now (2.13) and (2.3) followed by Young's inequality and then (3.5) yields

$$\begin{aligned}|(B(Q_\lambda u_2,P_\lambda u_2),AP_\lambda u_2)| &\leqslant c_1\,|Q_\lambda u_2|^{1/2}\,\|Q_\lambda u_2\|^{1/2}\,\|P_\lambda u_2\|^{1/2}\,|AP_\lambda u_2|^{3/2}\\ &\leqslant c_1\lambda^{-3/4}\,|AQ_\lambda u_2|\,\|P_\lambda u_2\|^{1/2}\,|AP_\lambda u_2|^{3/2}\\ &\leqslant \frac{2c_1^2}{\nu\lambda^{3/2}}\,\|P_\lambda u_2\|\,|AP_\lambda u_2|^3+\frac{\nu}{8}\,|AQ_\lambda u_2|^2\\ &\leqslant \frac{2c_1^2M_1^4}{\nu}+\frac{\nu}{8}\,|AQ_\lambda u_2|^2.\end{aligned}$$

The inequalities (2.13), (2.3), and (2.5) followed by Young's inequality and (3.5) yields

$$\begin{aligned}|(B(P_\lambda u_2,Q_\lambda u_2),AP_\lambda u_2)| &\leqslant c_1\,|P_\lambda u_2|^{1/2}\,\|P_\lambda u_2\|^{1/2}\,\|Q_\lambda u_2\|^{1/2}\,|AQ_\lambda u_2|^{1/2}\,|AP_\lambda u_2|\\ &\leqslant c_1\lambda^{-1/4}\,|P_\lambda u_2|^{1/2}\,\|P_\lambda u_2\|^{1/2}\,|AP_\lambda u_2|\,|AQ_\lambda u_2|\\ &\leqslant c_1\lambda^{-1/4}\lambda_1^{-1/4}\,\|P_\lambda u_2\|\,|AP_\lambda u_2|\,|AQ_\lambda u_2|\\ &\leqslant \frac{2c_1^2}{\nu\lambda^{1/2}\lambda_1^{1/2}}\,\|P_\lambda u_2\|^2\,|AP_\lambda u_2|^2+\frac{\nu}{8}\,|AQ_\lambda u_2|^2\\ &\leqslant \left(\frac{2c_1^2M_1^4}{\nu}\right)\frac{\lambda^{1/2}}{\lambda_1^{1/2}}+\frac{\nu}{8}\,|AQ_\lambda u_2|^2.\end{aligned}$$

Finally (2.13) and (2.3) followed by Young's inequality and (3.5) yields

$$\begin{aligned}|(B(Q_\lambda u_2,Q_\lambda u_2),AP_\lambda u_2)| &\leqslant c_1\,|Q_\lambda u_2|^{1/2}\,\|Q_\lambda u_2\|\,|AQ_\lambda u_2|^{1/2}\,|AP_\lambda u_2|\\ &\leqslant c_1\lambda^{-1/2}\,\|Q_\lambda u_2\|\,|AQ_\lambda u_2|\,|AP_\lambda u_2|\\ &\leqslant \frac{2c_1^2}{\nu\lambda}\,\|Q_\lambda u_2\|^2\,|AP_\lambda u_2|^2+\frac{\nu}{8}\,|AQ_\lambda u_2|^2\\ &\leqslant \frac{2c_1^2M_1^2}{\nu}\,\|Q_\lambda u_2\|^2+\frac{\nu}{8}\,|AQ_\lambda u_2|^2.\end{aligned}$$

It follows that (3.6) becomes

$$\frac{d}{dt}\|Q_\lambda u_2\|^2+\nu\,|AQ_\lambda u_2|^2\leqslant\frac{4c_1^2M_1^2}{\nu}\|Q_\lambda u_2\|^2+\frac{4}{\nu}|f|^2+\beta_1 \tag{3.7}$$

where the constant

$$\beta_1=\frac{4c_1^2M_1^4}{\nu}\left\{1+\frac{\lambda^{1/2}}{\lambda_1^{1/2}}\right\}.$$

Applying (2.3) to the second term on the left of (3.7) and regrouping yields

$$\frac{d}{dt}\|Q_\lambda u_2\|^2+\left\{\nu\lambda-\frac{4c_1^2M_1^2}{\nu}\right\}\|Q_\lambda u_2\|^2\leqslant\frac{4}{\nu}|f|^2+\beta_1.$$

This inequality may be written

$$\frac{d\xi}{dt}+\beta_2\xi\leqslant\frac{4}{\nu}|f|^2+\beta_1 \tag{3.8}$$

where

$$\beta_2=\nu\lambda-\frac{4c_1^2M_1^2}{\nu}\qquad\text{and}\qquad\xi=\|Q_\lambda u_2\|^2.$$

Gronwall's inequality applied to (3.8) yields that

$$\xi(t)\leqslant\xi(0)\,e^{-\beta_2 t}+\frac{\beta_1}{\beta_2}(1-e^{-\beta_2 t})+\frac{4}{\nu}\int_0^t|f(s)|^2\,e^{-\beta_2(t-s)}\,ds. \tag{3.9}$$

Since $f\in L^2_{\text{loc}}((0,\infty);H)$ it follows that $\|Q_\lambda u_2(t)\|^2$ is bounded for any interval $[0,T]$. Hence $u_2\in L^\infty((0,T);V)$.

Next we show $u_2\in L^2((0,T);D(A))$. Let M_2 be the bound exhibited above such that $\|u_2(t)\|^2\leqslant M_2$ for all t in $[0,T]$. Substituting this bound into (3.7) one obtains

$$\frac{d}{dt}\|Q_\lambda u_2\|^2+\nu\,|AQ_\lambda u_2|^2\leqslant\frac{4}{\nu}|f|^2+\beta_3 \tag{3.10}$$

where

$$\beta_3=\frac{4c_1^2M_1^2M_2^2}{\nu}+\beta_1.$$

Gronwall's inequality applied to (3.10) yields

$$\|Q_\lambda u_2(t)\|^2 + \nu \int_0^T |AQ_\lambda u_2|^2 \leqslant \|Q_\lambda u_2(0)\|^2 + \frac{4}{\nu}\int_0^T |f|^2 + T\beta_3.$$

Upon dropping the first term on the left and majorizing the first term on the right by M_2^2 it follows that

$$\int_0^T |AQ_\lambda u_2|^2 \leqslant \frac{1}{\nu}\left\{ M_2^2 + \frac{4}{\nu}\int_0^T |f|^2 + T\beta_3 \right\}.$$

Therefore $u_2 \in L^2((0, T); D(A))$.

The proof that $du_2/dt \in L^2((0, T); H)$ proceeds in exactly the same way as for the two-dimensional Navier–Stokes equations. The Galerkin method then leads to the existence of solutions to (3.1) satisfying (3.3).

Next, we show that such solutions are unique and depend continuously on the initial data. Let u_i and v_i be two solutions to (3.1) satisfying (3.3) for $i = 1, 2$ with initial conditions in V such that $P_\lambda u_1(0) = P_\lambda u_2(0)$ and $P_\lambda v_1(0) = P_\lambda v_2(0)$. Let the constants M_1 and M_2 be chosen large enough so that $\|u_i(t)\| \leqslant M_i$ and $\|v_i(t)\| \leqslant M_i$ for $i = 1, 2$ and almost every t in $[0, T]$. Let $w_i = u_i - v_i$. Since u_1 and v_1 are solutions to the standard two-dimensional Navier–Stokes equations, then Theorem 2.2 implies

$$\|w_1(t)\|^2 \leqslant \psi(t)\, \|w_1(0)\|^2 \qquad \text{for} \quad t \geqslant 0 \tag{3.11}$$

for some continuous monotone increasing function $\psi(t)$ with $\psi(0) = 1$. To obtain similar estimates on w_2, subtract the equation for v_2 from the equation for u_2. Thus,

$$\frac{dw_2}{dt} + \nu A w_2 = P_\lambda(B(v_1, v_1) - B(u_1, u_1)) + Q_\lambda(B(v_2, v_2) - B(u_2, u_2)).$$

Introducing $\mp P_\lambda B(v_1, u_1)$ and $\mp P_\lambda B(v_2, u_2)$ on the right side yields

$$\frac{dw_2}{dt} + \nu A w_2 = -P_\lambda(B(v_1, w_1) + B(w_1, u_1)) - Q_\lambda(B(v_2, w_2) + B(w_2, u_2)).$$

Since $w_2 \in L^2(0, T; D(A))$ and $dw_2/dt \in L^2(0, T; H)$ then the interpolation lemma of Lions–Magenes[36] implies that

$$\left(\frac{dw_2}{dt}, Aw_2\right) = \frac{1}{2}\frac{d}{dt}\|w_2\|^2.$$

See also Corollary 7.3 in ref. 39 or Lemma 1.2 in ref. 40. Now, taking inner products with Aw_2 and using the fact that $P_\lambda w_2 = P_\lambda w_1$ we obtain

$$\frac{1}{2}\frac{d}{dt}\|w_2\|^2 + \nu\,|Aw_2|^2 = -(B(v_1, w_1), P_\lambda Aw_1) - (B(w_1, u_1), P_\lambda Aw_1)$$
$$-(B(v_2, w_2), Q_\lambda Aw_2) - (B(w_2, u_2), Q_\lambda Aw_2). \quad (3.12)$$

By (2.12), (2.4), and (2.5) and then (3.11) we have

$$|(B(v_1, w_1), P_\lambda Aw_1)| \leqslant |v_1|^{1/2}\,\|v_1\|^{1/2}\,\|w_1\|\,|P_\lambda Aw_1|\,\|P_\lambda Aw_1\|$$
$$\leqslant \frac{\lambda^{3/2}}{\lambda_1^{1/2}}\,\|v_1\|\,\|w_1\|^2 \leqslant \frac{\lambda^{3/2}}{\lambda_1^{1/2}}\,M_1\psi(t)\,\|w_1(0)\|^2.$$

Similarly we estimate

$$|(B(w_1, u_1), P_\lambda Aw_1)| \leqslant |w_1|^{1/2}\,\|w_1\|^{1/2}\,\|u_1\|\,|P_\lambda Aw_1|\,\|P_\lambda Aw_1\|$$
$$\leqslant \frac{\lambda^{3/2}}{\lambda_1^{1/2}}\,\|u_1\|\,\|w_1\|^2 \leqslant \frac{\lambda^{3/2}}{\lambda_1^{1/2}}\,M_1\psi(t)\,\|w_1(0)\|^2.$$

Using (2.13), Young's inequality and then (2.5) we estimate

$$|(B(v_2, w_2), Q_\lambda Aw_2)| \leqslant |v_2|^{1/2}\,\|v_2\|^{1/2}\,\|w_2\|^{1/2}\,|Aw_2|^{3/2}$$
$$\leqslant \left(\frac{3}{2\nu}\right)^3 \frac{1}{4}\,|v_2|^2\,\|v_2\|^2\,\|w_2\|^2 + \frac{\nu}{2}\,|Aw_2|^2$$
$$\leqslant \frac{27}{32\nu^3}\,\frac{M_2^4}{\lambda_1}\,\|w_2\|^2 + \frac{\nu}{2}\,|Aw_2|^2$$

and also

$$|(B(w_2, u_2), Q_\lambda Aw_2)| \leqslant |w_2|^{1/2}\,\|w_2\|^{1/2}\,\|u_2\|^{1/2}\,|Au_2|^{1/2}\,|Aw_2|$$
$$\leqslant \frac{1}{2\nu}\,|w_2|\,\|w_2\|\,\|u_2\|\,|Au_2| + \frac{\nu}{2}\,|Aw_2|^2$$
$$\leqslant \frac{1}{2\nu}\,\lambda_1^{-1/2}\,\|w_2\|^2\,\|u_2\|\,|Au_2| + \frac{\nu}{2}\,|Aw_2|^2$$
$$\leqslant \frac{1}{4\nu}\,\|w_2\|^2\left\{M_2^2 + \frac{1}{\lambda_1}\,|Au_2|^2\right\} + \frac{\nu}{2}\,|Aw_2|^2.$$

Substituting these estimates into (3.12) we obtain

$$\frac{d}{dt}\|w_2\|^2 \leqslant \beta_4 \|w_1(0)\|^2 + \beta_5 \|w_2\|^2 \tag{3.13}$$

where

$$\beta_4(t) = 4\frac{\lambda^{3/2}}{\lambda_1^{1/2}} M_1 \psi(t) \qquad \text{and} \qquad \beta_5(t) = \frac{1}{2\nu}\left\{\frac{27M_2^4}{8\nu^2\lambda_1} + M_2^2 + \frac{1}{\lambda_1}|Au_2(t)|^2\right\}.$$

Gronwall's inequality applied to (3.13) yields that

$$\|w_2(t)\|^2 \leqslant \|w_2(0)\|^2 \exp\left\{\int_0^t \beta_5(s)\, ds\right\} + \|w_1(0)\|^2 \int_0^t \beta_4(\tau) \exp\left\{\int_\tau^t \beta_5(s)\, ds\right\} d\tau.$$

Since $u_2 \in L^2((0, T); D(A))$ then continuity with respect to the initial conditions follows. In particular, solutions of (3.1) satisfying (3.3) are unique. ∎

Note that the bounds in (3.9) are not uniform in time unless $\beta_2 > 0$. This implies that λ must be sufficiently large for us to prove that the system (3.1) is dissipative. A slightly sharper result than the one which results from the above observation appears as Theorem 3.5 at the end of this section.

The uniqueness given by Theorem 3.1 guarantees that if $u_1(t)$ and $u_2(t)$ happen to agree at some point in time, then they will remain equal for all subsequent times. In particular, if $\eta = Q_\lambda u_0$ then $u_1(t) = u_2(t)$ for all t. The following lemma establishes bounds on the convergence of continuous data assimilation in terms of time averages of the reference calculation u_1. As λ increases, the resolution of the measurements becomes finer. Therefore, we expect that $u_2(t)$ becomes a better and better approximation of $u_1(t)$ as $\lambda \to \infty$.

Lemma 3.2. Let $u_1(t)$ and $u_2(t)$ be the unique strong solutions to (3.1) with $u_0 = u_1(0) \in V$, $\eta = Q_\lambda u_2(0) \in Q_\lambda V$, and $f \in L^2_{\text{loc}}((0, \infty); H)$ given by Theorem 3.1. Then

$$|u_1(t) - u_2(t)|^2 \leqslant |u_1(0) - u_2(0)|^2 \exp\left\{-\nu\lambda t + \frac{c_1^2}{\nu}\int_0^t \|u_1(\tau)\|^2\, d\tau\right\} \tag{3.14}$$

and

$$\|u_1(t) - u_2(t)\|^2 \leqslant \|u_1(0) - u_2(t)\|^2 \exp\left\{-\nu\lambda t + \frac{c_1^2}{\nu\lambda}\int_0^t |Au_1(\tau)|^2\, d\tau\right\}. \tag{3.15}$$

Proof. Let $\delta = u_1 - u_2$. Subtract the second equation in (3.1) from the first to obtain

$$\frac{d\delta}{dt} + \nu A\delta + Q_\lambda(B(u_1, u_1) - B(u_2, u_2)) = 0. \tag{3.16}$$

Introduce $\mp Q_\lambda B(u_2, u_1)$ and further introduce $\pm Q_\lambda B(u_1, \delta)$ into (3.16) to obtain

$$\frac{d\delta}{dt} + \nu A\delta + Q_\lambda(B(\delta, u_1) + B(u_1, \delta) - B(\delta, \delta)) = 0. \tag{3.17}$$

We shall make two estimates showing the convergence of δ to zero. First, we find conditions under which $|\delta(t)| \to 0$ as $t \to \infty$, and second, we find conditions under which $\|\delta(t)\| \to 0$ as $t \to \infty$.

We obtain estimates on $|\delta|$ by multiplying (3.17) by δ and integrating. Since $Q_\lambda \delta = \delta$ it follows from (2.8) that

$$\frac{1}{2}\frac{d}{dt}|\delta|^2 + \nu\|\delta\|^2 + (B(\delta, u_1), \delta) = 0. \tag{3.18}$$

Inequality (2.12) followed by Young's inequality yields

$$|(B(\delta, u_1), \delta)| \leqslant c_1 |\delta| \|\delta\| \|u_1\| \leqslant \frac{c_1^2}{2\nu}|\delta|^2 \|u_1\|^2 + \frac{\nu}{2}\|\delta\|^2. \tag{3.19}$$

Substituting (3.19) into (3.18) one obtains

$$\frac{d}{dt}|\delta|^2 + \nu\|\delta\|^2 \leqslant \frac{c_1^2}{\nu}|\delta|^2 \|u_1\|^2.$$

Applying (2.3) to the second term on the left yields

$$\frac{d}{dt}|\delta|^2 + \left\{\nu\lambda - \frac{c_1^2}{\nu}\|u_1\|^2\right\}|\delta|^2 \leqslant 0. \tag{3.20}$$

Now, Gronwall's inequality yields

$$|\delta(t)|^2 \leqslant |\delta(0)|^2 \exp\left\{-\nu\lambda t + \frac{c_1^2}{\nu}\int_0^t \|u_1(\tau)\|^2 \, d\tau\right\}.$$

Next, we obtain estimates on $\|\delta\|$ by taking the L^2 inner product of (3.17) with $A\delta$. Since $Q_\lambda A\delta = A\delta$ it follows from (2.9) that

$$\frac{1}{2}\frac{d}{dt}\|\delta\|^2 + \nu\,|A\delta|^2 + (B(u_1, \delta), A\delta) + (B(\delta, u_1), A\delta) = 0.$$

Further applying (2.10) one obtains

$$\frac{1}{2}\frac{d}{dt}\|\delta\|^2 + \nu\,|A\delta|^2 = (B(\delta, \delta), Au_1). \tag{3.21}$$

Estimate using (2.12) followed by (2.3) and then Young's inequality as

$$\begin{aligned}|(B(\delta, \delta), Au_1)| &\leqslant c_1\,|\delta|^{1/2}\,\|\delta\|\,|A\delta|^{1/2}\,|Au_1| \\ &\leqslant c_1\lambda^{-1/2}\,\|\delta\|\,|A\delta|\,|Au_1| \\ &\leqslant \frac{c_1^2}{2\nu\lambda}\,\|\delta\|^2\,|Au_1|^2 + \frac{\nu}{2}\,|A\delta|^2.\end{aligned}$$

Then substitute this estimate into (3.21) to obtain

$$\frac{d}{dt}\|\delta\|^2 + \nu\,|A\delta|^2 \leqslant \frac{c_1^2}{\nu\lambda}\,\|\delta\|^2\,|Au_1|^2.$$

Applying (2.3) to the second term on the left yields

$$\frac{d}{dt}\|\delta\|^2 + \left\{\nu\lambda - \frac{c_1^2}{\nu\lambda}\,|Au_1|^2\right\}\|\delta\|^2 \leqslant 0. \tag{3.22}$$

Now, Gronwall's inequality yields

$$\|\delta(t)\|^2 \leqslant \|\delta(0)\|^2 \exp\left\{-\nu\lambda t + \frac{c_1^2}{\nu\lambda}\int_0^t |Au_1(\tau)|^2\,d\tau\right\}.$$

This finishes the proof of the lemma. ∎

Combining Lemma 3.2 with Lemma 2.4 we obtain rigorous conditions on λ in terms of f and ν which ensure that continuous data assimilation works. Namely, we prove the following version of Theorem 1.5.

Theorem 3.3. Let

$$M_1 = \left\{\sup_{t>0}\frac{1}{t}\int_0^t \|f(\tau)\|_*^2\,d\tau\right\}^{1/2} \quad \text{and} \quad M_2 = \left\{\sup_{t>0}\frac{1}{t}\int_0^t |f(\tau)|^2\,d\tau\right\}^{1/2}.$$

Then, given a bounded subset $B_0 \subset V$ and $f \in L^2_{\mathrm{loc}}((0,T);H)$ with $M_2 < \infty$, there exists K_1 and K_2 large enough such that for every $u_0 = u_1(0) \in B_0$ and $\eta = Q_\lambda u_2(0) \in Q_\lambda V$ the solutions $u_1(t)$ and $u_2(t)$ to (3.1) satisfy

(i) If there exists α such that $0 < 2\alpha \leqslant \nu\lambda - c_1^2 \nu^{-3} M_1^2$ then

$$|u_1(t) - u_2(t)| \leqslant |u_1(0) - u_2(0)|\, K_1 e^{-\alpha t} \qquad \text{for} \quad t \geqslant 0.$$

(ii) If there exists α such that $0 < 2\alpha \leqslant \nu\lambda - c_1^2 (\nu^3\lambda)^{-1} M_2^2$ then

$$\|u_1(t) - u_2(t)\| \leqslant \|u_1(0) - u_2(0)\|\, K_2 e^{-\alpha t} \qquad \text{for} \quad t \geqslant 0.$$

Proof. Let $\delta = u_1 - u_2$. To estimate $|\delta(t)|$ substitute (2.14) from Lemma 2.4 into (3.14) from Lemma 3.2 to obtain

$$\begin{aligned} |\delta(t)|^2 &\leqslant |\delta(0)|^2 \exp\left\{ -\nu\lambda t + \frac{t c_1^2}{\nu} \left(\frac{1}{\nu t} |u_0|^2 + \frac{1}{\nu^2} M_1^2 \right) \right\} \\ &\leqslant |\delta(0)|^2 \exp\left\{ \frac{c_1^2}{\nu^2} |u_0|^2 \right\} \exp\left\{ \left(-\nu\lambda + \frac{c_1^2}{\nu^3} M_1^2 \right) t \right\}. \end{aligned}$$

It follows that, if $0 < 2\alpha \leqslant \nu\lambda - c_1^2 \nu^{-3} M_1^2$ then $|\delta(t)| \leqslant |\delta(0)|\, K_1 e^{-\alpha t}$ where K_1 is chosen large enough such that

$$K_1 \geqslant \exp\left\{ \frac{c_1^2}{2\nu^2} |u_0|^2 \right\} \qquad \text{for all} \quad u_0 \in B_0.$$

To estimate $\|\delta(t)\|$ substitute (2.15) from Lemma 2.4 into (3.15) from Lemma 3.2 to obtain

$$\begin{aligned} \|\delta(t)\|^2 &\leqslant \|\delta(0)\|^2 \exp\left\{ -\nu\lambda t + \frac{t c_1^2}{\nu\lambda} \left(\frac{1}{\nu t} \|u_0\|^2 + \frac{1}{\nu^2} M_2^2 \right) \right\} \\ &\leqslant \|\delta(0)\|^2 \exp\left\{ \frac{c_1^2}{\nu^2\lambda} \|u_0\|^2 \right\} \exp\left\{ \left(-\nu\lambda + \frac{c_1^2}{\nu^3\lambda} M_2^2 \right) t \right\}. \end{aligned}$$

It follows that, if $0 < 2\alpha \leqslant \nu\lambda - c_1^2 (\nu^3\lambda)^{-1} M_2^2$ then $\|\delta(t)\| \leqslant \|\delta(0)\|\, K_2 e^{-\alpha t}$ where K_2 is chosen large enough such that

$$K_2 \geqslant \exp\left\{ \frac{c_1^2}{2\nu^2\lambda} \|u_0\|^2 \right\} \qquad \text{for all} \quad u_0 \in B_0.$$

This finishes the proof. ∎

Corollary 3.4. Under the hypothesis of Theorem 3.3 the approximation u_2 converges to u_1 in $L^\infty([0,\infty];V)$ as $\lambda \to \infty$.

Proof. Since K_2 in Theorem 3.3 may be chosen independently of λ then

$$\|u_1(t)-u_2(t)\| \leqslant \|u_1(0)-u_2(0)\| K_2 e^{-\alpha t} \leqslant K_2 \|Q_\lambda(u_0-\eta)\| \to 0$$

as $\lambda \to \infty$. ∎

Proof of Theorem 1.5. Notice in the case f is time-independent that $M_1 = \|f\|_*$ and $M_2 = |f|$ in Theorem 3.3. The proof of Theorem 1.5 then follows from Theorem 3.3 and the fact that the global attractor of (2.6) is bounded in V. ∎

Note that any bounds on the critical value of λ for which continuous data assimilation works must remain invariant under the scaling presented in (1.8) in order to be sharp. Since all wave numbers in the original Fourier space are doubled upon setting $\tilde{u}_1(x,t) = 2u_1(2x,4t)$ and $\tilde{f}(x) = 8f(2x)$, then the observational measurements $P_{\tilde{\lambda}}\tilde{u}_1(t)$ are equivalent to $P_\lambda u_1(t)$ exactly when $\tilde{\lambda} = 4\lambda$.

Assume, first, that there is a bound on λ in terms of $\|f\|_*$ which is sharp. In particular, suppose $\lambda \sim C\|f\|_*^\beta$ for some constants C and β. Since $\|\tilde{f}\|_* = 4\|f\|_*$ then rewriting $\tilde{\lambda} \sim C\|\tilde{f}\|_*^\beta$ in terms of λ and f yields $4\lambda \sim 4^\beta C|f|^\beta$. It follows that $\beta = 1$ and therefore $\lambda \sim C\|f\|_*$. However, the first bound in Theorem 3.3 depends on $\|f\|_*^2$, therefore it could not be sharp. Similarly, if $\lambda \sim C|f|^\beta$, then rescaling $\tilde{\lambda} \sim C|\tilde{f}|^\beta$ yields $4\lambda \sim C8^\beta|\tilde{f}|^\beta$. It follows, in this case, that $\beta = 2/3$ and so $\lambda \sim C|f|^{2/3}$. Thus, both of the results in Theorem 3.3 are only upper bounds.

We end this section with a result on the dissipativity of the continuous data assimilation equations (3.1). Whether this system of equations is dissipative for all, in particular smaller, values of λ appears to be an interesting open question.

Theorem 3.5. Given forcing $f \in H$ and provided that λ satisfies (1.10), then the system of equations (3.1) is dissipative and has an absorbing ball in V.

Proof. Since u_1 satisfies the usual two-dimensional Navier–Stokes equations with forcing $f \in H$ then it has an absorbing ball in V. See, for example, refs. 9, 16, 39, or 40 and 41. For u_2 we use Theorem 3.3 to estimate f_2 and use that estimate to find an absorbing ball.

Let $\delta(t) = u_1(t) - u_2(t)$. Then (2.4) implies

$$\begin{aligned} |f_1 - f_2| &\leqslant |P_\lambda B(u_2, u_2) - P_\lambda B(u_1, u_1)| \\ &\leqslant |P_\lambda B(\delta, \delta)| + |P_\lambda B(u_1, \delta)| + |P_\lambda B(\delta, u_1)| \\ &\leqslant \lambda^{3/2}\{\|B(\delta, \delta)\|_{-3} + \|B(u_1, \delta)\|_{-3} + \|B(\delta, u_1)\|_{-3}\}. \end{aligned}$$

For $w \in V_3$ the Sobolev embedding $\|\nabla w\|_{L^\infty} \leqslant C \|w\|_3$ yields the estimates

$$|\langle B(\delta, \delta), w\rangle| = |\langle B(\delta, w), \delta\rangle| \leqslant \|\nabla w\|_{L^\infty} |\delta|^2 \leqslant C \|w\|_3 |\delta|^2$$

$$|\langle B(u_1, \delta), w\rangle| = |\langle B(u_1, w), \delta\rangle| \leqslant \|\nabla w\|_{L^\infty} |u_1| |\delta| \leqslant C \|w\|_3 |u_1| |\delta|$$

$$|\langle B(\delta, u_1), w\rangle| = |\langle B(\delta, w), u_1\rangle| \leqslant \|\nabla w\|_{L^\infty} |u_1| |\delta| \leqslant C \|w\|_3 |u_1| |\delta|.$$

If λ satisfies inequality (1.10) then Theorem 3.3 implies $|\delta(t)| \to 0$ as $t \to \infty$. Thus,

$$|f_1 - f_2| \leqslant C\lambda^{3/2}\{|\delta|^2 + 2|u_1| |\delta|\} \to 0 \qquad \text{as} \quad t \to \infty. \tag{3.23}$$

This implies that f_2 has the same asymptotic bounds in time as f.

Now, Theorem 3.3 implies that for any bounded subset $B_0 \subset V$ there exists a time $s > 0$ such that for every $u_0 \in B_0$ and $\eta \in Q_\lambda V$ the corresponding f_2 obeys

$$|f_2(t)| \leqslant 2|f| \qquad \text{for} \quad t > s.$$

Let

$$B_1 = \{u_2(s) : u_0 \in B_0 \text{ and } \eta \in Q_\lambda B_0\}.$$

Continuous dependence on the initial data given by Theorem 3.1 implies that B_1 is bounded in V. Denote that bound by M_1. We now estimate $\|u_2(t)\|$.

Multiply the second equation in (3.1) by Au_2 to obtain

$$\frac{1}{2}\frac{d}{dt}\|u_2\|^2 + \nu |Au_2|^2 = (f_2, Au_2).$$

Applying Cauchy–Schwarz and Young's inequalities gives

$$\frac{d}{dt}\|u_2\|^2 + \nu |Au_2|^2 = \frac{1}{\nu}|f_2|^2.$$

Applying the Poincaré inequality (2.5) to the second term on the right yields

$$\frac{d}{dt}\|u_2\|^2+\nu\lambda_1\|u_2\|^2=\frac{1}{\nu}|f_2|^2$$

and integrating over the interval $[s, t]$ one obtains

$$\|u_2(t)\|^2\leqslant\|u_2(s)\|^2 e^{-\nu\lambda_1(t-s)}+\frac{1}{\nu}\int_s^t e^{-\nu\lambda_1(t-\tau)}|f_2(\tau)|^2\,d\tau$$

$$\leqslant M_1^2 e^{-\nu\lambda_1(t-s)}+\frac{2|f|^2}{\nu^2\lambda_1}\{1-e^{-\nu\lambda_1(t-s)}\}.$$

Therefore, there exists $T>s$ large enough such that for every $u_0\in B_0$ and $\eta\in Q_\lambda B_0$ the solution u_2 to the second equation in (3.1) satisfies

$$\|u_2(t)\|^2\leqslant\frac{3|f|^2}{\nu^2\lambda_1}\qquad\text{for}\quad t>T.$$

Thus, Eqs. (3.1) are dissipative. ▮

Note that (3.23) shows in the case of continuous data assimilation that $|u_1(t)-u_2(t)|\to 0$ as $t\to\infty$ implies $|f_1(t)-f_2(t)|\to 0$ as $t\to\infty$. This same implication does not hold for two solutions u_1 and u_2 of the Navier–Stokes equations with respective time-dependent forcing functions f_1 and f_2 in general. Consider the following simple example. Let

$$u_1=\begin{pmatrix}0\\(t+1)^{-1}\sin(t+1)^2\end{pmatrix}\cos(x)$$

and

$$u_2=\begin{pmatrix}(t+1)^{-1}\cos(t+1)^2\\0\end{pmatrix}\cos(y).$$

Then u_1 and u_2 are solutions of (2.6) with

$$f_1=\begin{pmatrix}0\\2\cos(t+1)^2-(t+1)^{-2}\sin(t+1)^2+\nu(t+1)^{-1}\sin(t+1)^2\end{pmatrix}\cos(x)$$

and

$$f_2=\begin{pmatrix}-2\sin(t+1)^2-(t+1)^{-2}\cos(t+1)^2+\nu(t+1)^{-1}\cos(t+1)^2\\0\end{pmatrix}\cos(y).$$

Clearly $\|u_1(t)-u_2(t)\|_\alpha \to 0$ as $t \to \infty$ for any α, however

$$|f_1-f_2|^2 = |f_1|^2+|f_2|^2 \sim 4 \qquad \text{as} \quad t \to \infty.$$

Therefore, $|f_1(t)-f_2(t)|$ need not converge to zero as $t \to \infty$ even though $\|u_1(t)-u_2(t)\|_\alpha \to 0$ as $t \to \infty$ for any α. This implies that Theorems 1.4, 1.5, and 3.3 cover situations where the hypothesis of Theorem 1.3 are violated. Similar examples can be constructed using spatial oscillations whose length scales decrease over time. For these examples $\|u_1-u_2\| \to 0$, but $|Q_\lambda f_1 - Q_\lambda f_2|$ does not converge to zero for any λ.

4. NUMERICAL RESULTS

In this section we study numerically how the length scales present in the forcing function f affect the rate of continuous data assimilation and the number of determining modes. It is worth mentioning that almost all the previous analytical studies concerning the number of degrees of freedom in turbulent flow have focused on the Grashof number and almost none have addressed the effect of the spatial structure of the forcing on the dynamics. However, there were some computational results that took the structure of the forcing into consideration. See, for example, the work of Marchioro,[37] Jolly,[29] Platt *et al.*,[38] and references therein.

Let $\mathscr{G}(R)$ and $\mathscr{F}(\lambda_f)$ be as given in the introduction. Thus, $\mathscr{G}(R)$ is the set of all time-independent forcing functions f with Grashof number $\mathrm{Gr}(f) = R$ and $\mathscr{F}(\lambda_f)$ is the subset of $\mathscr{G}(R)$ consisting of the time-independent forcing functions that are supported on an annulus in Fourier space centered at λ_f of the form (1.11). All computational experiments were performed with $\nu = 0.0001$ and $\eta = 0$ on the 2π-periodic torus for forcing functions with a Grashof number of $R = 250000$. Our computational results consist of two sets of experiments.

For our first experiment we select functions from $\mathscr{F}(\lambda_f)$ for values of λ_f ranging from 25 through 625. We work in the vorticity representation. Thus, any $f \in \mathscr{F}(\lambda_f)$ may be specified in terms of $g = \nabla \times f$ according to

$$\hat{f}_k = \frac{\hat{g}_k}{k_1^2+k_2^2}\begin{bmatrix} -ik_2 \\ ik_1 \end{bmatrix} \qquad \text{where} \quad g = \sum_{\lambda_m \leqslant |k|^2 \leqslant \lambda_M} \hat{g}_k \phi_k. \tag{4.1}$$

To obtain a representative function $f \in \mathscr{F}(\lambda_f)$ for each value of λ_f under consideration, we take the Fourier coefficients g_k to be Gaussian distributed, subject to the reality condition $\hat{g}_k = \overline{\hat{g}_{-k}}$ and normalized so that $|f| = 0.0025$.

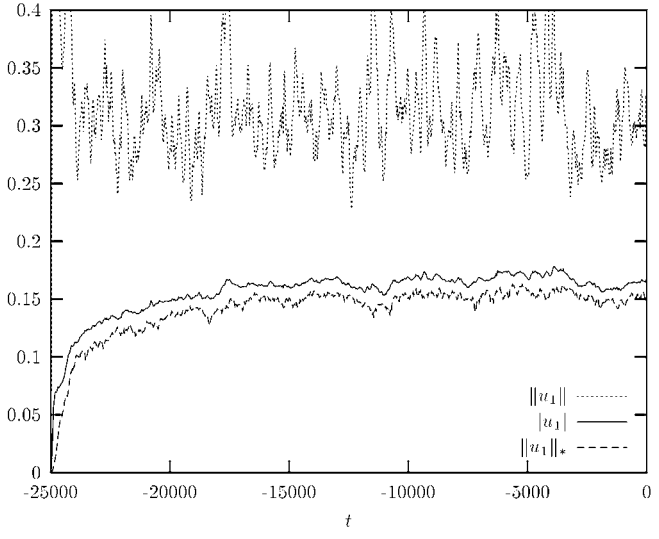

Fig. 1. Evolution of $\|u_1\|$, $|u_1|$, and $\|u_1\|_*$ for $\lambda_f = 25$ shows that initial data for the continuous data assimilation experiment is very close to the global attractor.

The initial condition u_0 for each continuous data assimilation experiment was chosen so that it faithfully reflects the long term energetics of the forcing. This was done by integrating the Navier–Stokes equations (2.6) starting at time $t = -25000$ with $u_1(-25000) = 0$ until time $t = 0$. Figure 1 shows the time evolution of $\|u_1\|$, $|u_1|$, and $\|u_1\|_*$ for a forcing function with $\lambda_f = 25$. By the end of the run these quantities have reached their statistically stationary states. Thus, one can assume that $u_0 = u_1(0)$ is on the attractor. We note that as long as u_0 reflects the long term energetics of the forcing the exact method of its choice is not important.

Given a particular forcing function and initial condition u_0 the data assimilation parameter λ for P_λ in (3.1) was then varied to determine its effect on the time evolution of $\|u_1 - u_2\|$. As suggested by the bounds in Theorem 3.3 and illustrated in Fig. 2, convergence, when it occurs, is exponential in time. Although convergence is not always monotonic, it is, on average, exponential. Therefore, a least squares fit of $A\exp(-\alpha t)$ to $\|u_1 - u_2\|$ was made for each computation to obtain the rate of continuous data assimilation α. Values of α as a function of λ are given in Fig. 3 for the experiments with $\lambda_f \leqslant 361$ and in Fig. 4 for the experiments with $\lambda_f \geqslant 361$.

To provide a definite numerical criterion for deducing the number of determining modes, let λ_c be the smallest value of λ for which the corresponding rate of continuous data assimilation α satisfies $\alpha \geqslant 0.0005$. We take the number of determining modes N_c to be the rank of P_λ for $\lambda = \lambda_c$.

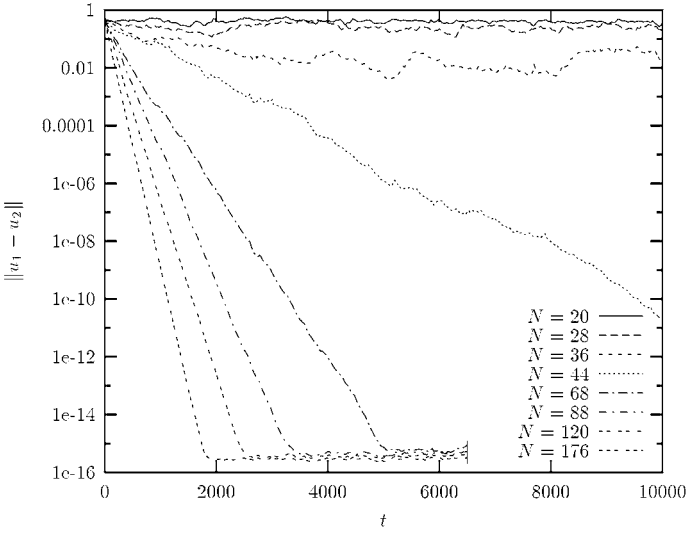

Fig. 2. Evolution of $\|u_1 - u_2\|$ with $\lambda_f = 64$ for continuous data assimilation on N Fourier modes. Convergence, when it occurs, is exponential in time.

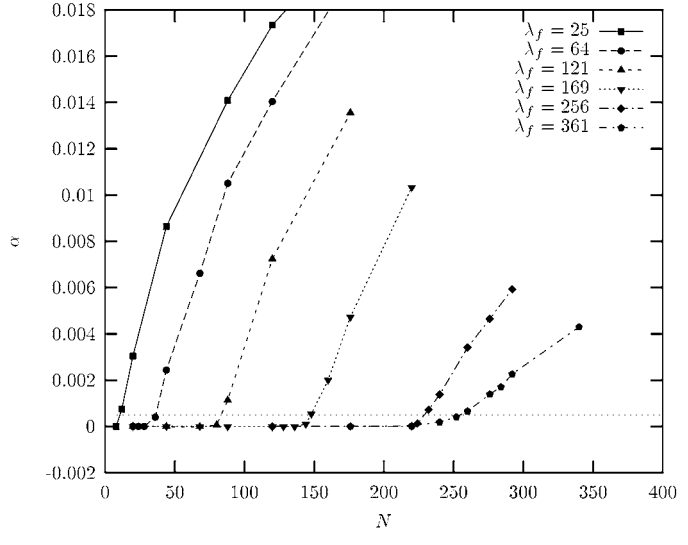

Fig. 3. Rate of continuous data assimilation for forcing supported on length scales between $\lambda_f = 25$ and 361. The horizontal line at $\alpha = 0.0005$ represents the cutoff for deducing the number of determining modes.

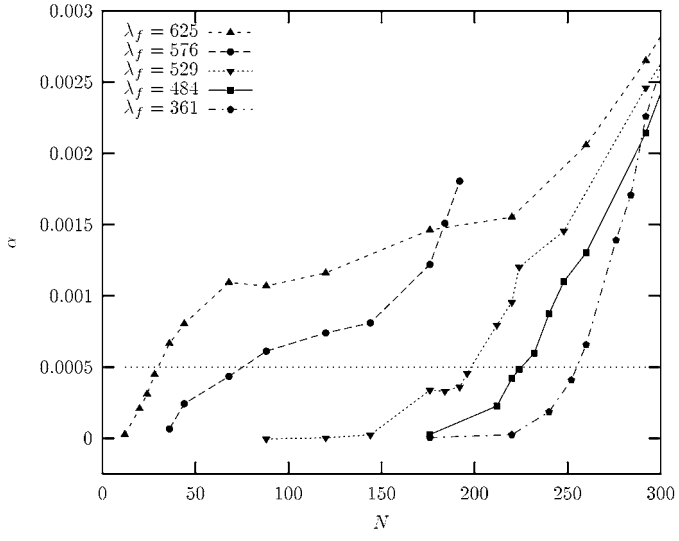

Fig. 4. Rate of continuous data assimilation for forcing supported on length scales between $\lambda_f = 361$ and 625. The horizontal line at $\alpha = 0.0005$ represents the cutoff for deducing the number of determining modes.

Table I summarizes how the number of determining modes depends on the length scales present in the forcing. Notice that the number of determining modes increases as λ_f increases from 25 through 361 but then decreases as λ_f increases from 361 through 625. We remark that the distances between successive values of λ_f have been chosen to be spaced far enough apart to guarantee that $\|f\|_*$ will decrease monotonically as λ_f increases.

To compare these results with our theory, substitute (1.12) into (1.10) and use the bounds on c_1 given in Lemma 2.3 to obtain

$$\begin{aligned}\lambda_c &\leqslant \min\{c_1^2 \nu^{-4} \|f\|_*^2, c_1 \nu^{-2} |f|\} \\ &\leqslant c_1 \nu^{-2} |f| \min\{c_1 \nu^{-2} |f| (\lambda_f^{1/2} - 1)^{-2}, 1\} \\ &\leqslant 539789 \min\{539789 (\lambda_f^{1/2} - 1)^{-2}, 1\}.\end{aligned}$$

Table I. The Relationship between the Parameter λ_f in the Forcing, λ_c, and the Number of Determining Modes N_c

λ_f	25	64	121	169	256	361	484	529	576	625
λ_c	4	13	26	49	73	82	73	65	27	10
N_c	12	44	88	148	232	260	232	212	88	36

Hence, when $\lambda_f \geqslant 541260$ the first term in the minimum dominates, and our analytical bound on λ_c and consequently on N_c decreases as λ_f increases. In particular, our analytical estimate on the number of determining modes reaches zero for λ_f large enough. Although our computational estimates are much smaller and start decreasing long before our theoretical bounds do, it seems reasonable that the observed decrease in number of determining modes when forcing on smaller and smaller scales is still explained by the smallness of the V' norm of f when λ_f is large.

Something unexplained by our analysis appears to be happening for values of λ_f between 25 and 361. The number of determining modes increases as λ_f increases. In an intuitive sense, this can be seen as an extrapolation of the fact that when $\lambda_f = 0.7$ Theorem 1.7 implies that the dynamics are trivial. To shed further light on this case let us first examine the energy spectra of the reference calculations. Let

$$E(r) = L^2 \sum_{k \in \mathscr{J}_r} |\hat{u}_k|^2$$

where $\mathscr{J}_r = \{k \in \mathscr{J} : r - 1/2 < |k| \leqslant r + 1/2\}$ and define

$$\langle E(r) \rangle = \lim_{T \to \infty} \frac{1}{T} \int_0^T E(r)\, dt.$$

The average energy spectrum of the reference calculation u_1 corresponding to each of the forcing functions in Table I is shown in Fig. 5. Here we have estimated the limit at $T \to \infty$ by taking $T = 10000$. Note that as λ_f increases, the amount of energy in the high modes increases and a peak around λ_f becomes apparent. Also note that the total energy in the low modes decreases as λ_f increases.

Thus, there are two plausible explanations for the observed increase in the number of determining modes as λ_f ranges from 25 to 361. This increase might be caused by an increases of energy in the high modes of u_1 or it might be caused by a decrease of energy in the low modes. If we suppose that the small scales are generated from the large scales, then a decrease of energy in the low modes would leave less large scale motion to generate the small scales, and therefore lead to an increase in the number of determining modes. To test this hypothesis a second set of experiments was conducted.

Given $f_L \in \mathscr{F}(25)$ and $f_H \in \mathscr{F}(484)$ we set $f = \theta_L f_L + \theta_H f_H$ where $\theta_L^2 + \theta_H^2 = 1$. In this way we obtain forcing functions that are supported on two disjoint annuli in Fourier space—one on small wave numbers, the other on large. Here θ_L and θ_H are parameters determining the relative

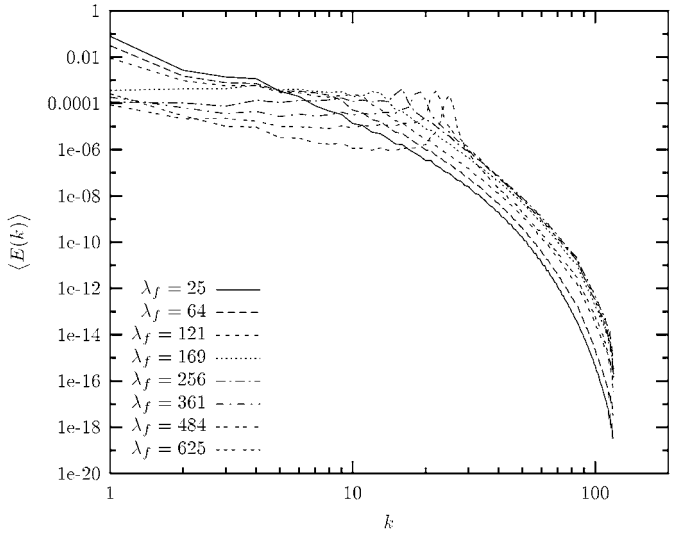

Fig. 5. Time averages of the energy spectrum of u_1 show a characteristic peak around λ_f for forcing functions supported on small length scales. The average was computed by taking $T = 10000$.

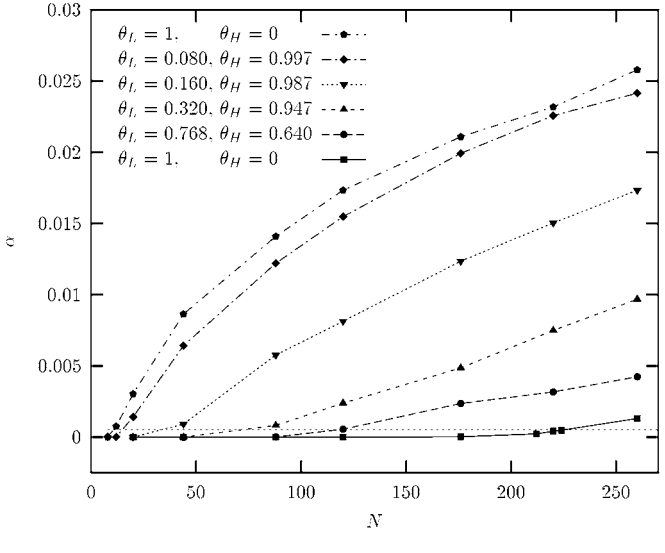

Fig. 6. Rate of continuous data assimilation for the forcing function $f = \theta_L f_L + \theta_H f_H$ where $f_L \in \mathscr{F}(25)$ and $f_H \in \mathscr{F}(484)$. The horizontal line at $\alpha = 0.0005$ represents the cutoff for deducing the number of determining modes.

Table II. The Relationship between the Weights θ_L and θ_H in the Forcing, λ_c, and the Number of Determining Modes N_c

θ_L	0	0.080	0.160	0.320	0.768	1
θ_H	1	0.997	0.987	0.947	0.640	0
λ_c	73	37	26	13	5	4
N_c	232	120	88	44	20	12

weights of the large and small length scales in the forcing. When θ_H is close to zero f may be viewed as the perturbation of the large scales f_L by the small scales f_H; when θ_L is close to zero f is the perturbation of the small scales f_H by the large scales f_L. The values of α for these computations are presented graphically in Fig. 6. Table II indicates how the number of determining modes depends on θ_L and θ_H. Note that the perturbation of the large scales f_L by the small scales f_H does not significantly change the number of determining modes, whereas the perturbation of the small scales f_H by the large scales f_L dramatically affects the number of determining modes. This is consistent with our hypothesis that it is the absence of the large scales in the forcing which are primarily responsible for the increase in number of determining modes as λ_f ranges from 25 through 361 in the first set of experiments.

Further evidence in support of this hypothesis may be obtained by examining the averaged energy spectrum in Fig. 7 of the reference calculation u_1 corresponding to each of the forcing functions in Table II. The most dramatic changes in the number of determining modes corresponds primarily to changes in the energy of the low modes of the energy spectrum.

It is amusing to note that the first three columns in Table II are qualitatively unchanged by taking $\theta_H = 1$ in each of them. In this case we obtain a sequence of forcing functions that increases in all norms while at the same time the corresponding number of determining modes decrease. A discussion of this seeming paradox and an explanation for it in terms of a Reynolds number based on the observational measurements $P_\lambda u_1(t)$ shall be explored, if efficable, in a future work.

5. COMPUTATIONAL METHODS

Numerical computations for this paper were carried out using a C code written by the authors in conjunction with the Fourier transform library of Frigo and Johnson.[26] The actual calculations were made on microcomputers running the GNU/Linux operating system and LAM/MPI at the University of Nevada, Reno and at the University of

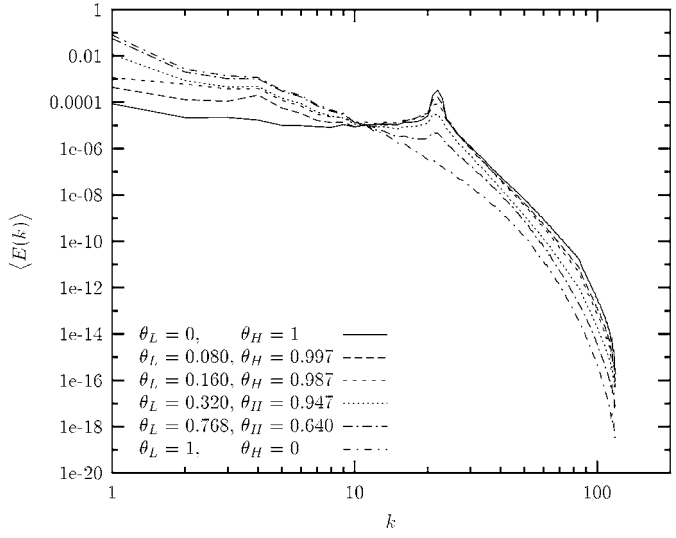

Fig. 7. Time averages of the energy spectrum of u_1 for $f = \theta_L f_L + \theta_H f_H$ where $f_L \in \mathscr{F}(25)$ and $f_H \in \mathscr{F}(484)$. The average was computed by taking $T = 10000$.

California, Irvine. Correct behavior of our code was verified by comparison to existing programs written by Mike Jolly and Stephen Montgomery.

We use a spectral Galerkin method and compute the two-dimensional incompressible Navier–Stokes equations in its vorticity form

$$\frac{\partial \omega}{\partial t} - \nu \Delta \omega + (u \cdot \nabla)\, \omega = g \tag{5.1}$$

where $\omega = \nabla \times u$ and $g = \nabla \times f$. Note that the one-third rule was used to avoid aliasing, see Canuto *et al.*[3] In terms of its Fourier decomposition (5.1) becomes

$$\frac{d\hat{\omega}_k}{dt} + \nu |k|^2 \hat{\omega}_k + ik \cdot \widehat{u\omega}_k = \hat{g}_k. \tag{5.2}$$

Following Henshaw, Kreiss, and Reyna in ref. 27, we integrate the dissipative term explicitly to obtain

$$\frac{d}{dt}\{\hat{\omega}_k \exp(\nu |k|^2 t)\} + ik \cdot \widehat{u\omega}_k \exp(\nu |k|^2 t) = \hat{g}_k \exp(\nu |k|^2 t) \tag{5.3}$$

and then integrate the remaining terms using a third order Adams–Bashforth scheme. Initial time steps are computed via a fourth order Runge–Kutta scheme.

Let $\hat{w}^j$ denote the Fourier transformed vorticity at time $t_j = j\,\Delta t$. Let

$$\Lambda = \mathrm{diag}(..., \nu(k_1^2 + k_2^2), ...)$$

and

$$F(t, \hat{w}) = -ik \cdot \widehat{u\omega}_k + \hat{g}_k.$$

Using these notations, the fourth order Runge–Kutta scheme used in our calculations may be written

$$\begin{aligned}
K_1 &= F(t_j, \hat{w}^j) \\
K_2 &= F(t_j + \Delta t/2,\ e^{-\Lambda \Delta t/2}(\hat{w}^j + K_1\,\Delta t/2)) \\
K_3 &= F(t_j + \Delta t/2,\ e^{-\Lambda \Delta t/2}\hat{w}^j + K_2\,\Delta t/2) \\
K_4 &= F(t_j + \Delta t,\ e^{-\Lambda \Delta t}\hat{w}^j + e^{-\Lambda \Delta t/2}K_3\,\Delta t) \\
\hat{w}^{j+1} &= e^{-\Lambda \Delta t}\hat{w}^j + (\Delta t/6)(e^{-\Lambda \Delta t}K_1 + 2e^{-\Lambda \Delta t/2}(K_2 + K_3) + K_4)
\end{aligned}$$

and the third order Adams–Bashforth scheme may be written

$$\begin{aligned}
\hat{w}^{j+1} = e^{-\Lambda \Delta t}\hat{w}^j + \frac{\Delta t}{12}\{&23e^{-\Lambda \Delta t}F(t_j; \hat{w}^j) - 16e^{-2\Lambda \Delta t}F(t_{j-1}, \hat{w}^{j-1}) \\
&+ 5e^{-3\Lambda \Delta t}F(t_{j-2}, \hat{w}^{j-2})\}.
\end{aligned}$$

In our analysis, the forcing function f and the dynamical equations governing the evolution of u_1 were assumed to be known exactly. Furthermore, the observable measurements $P_\lambda u_1(t)$ were assumed to be error free. Therefore, if $u_1(t)$ and $u_2(t)$ happen to be equal at any time t, then they will remain equal for all subsequent times.

We would like our numerical computations to reflect these assumptions as closely as possible. To ensure our computations of u_1 and u_2 are identical, we discretize the equations governing u_1 and u_2 in exactly the same way and use the same executable program to compute each solution. This avoids any variations in automatic compile-time optimizations. Furthermore, we explicitly specify the processor dependent run-time optimizations used by the Fourier transform library.[26] Additional care was taken when implementing the continuous data assimilation to ensure that the exact values of $P_\lambda u_1$ were used in a way that doesn't affect the discrete

dynamics. Thus, since we are using a three step method for the time integrator, if the numerical solutions $u_1(t)$ and $u_2(t)$ are bit for bit equal at any three consecutive times t_j, t_{j-1}, and t_{j-2}, then they will remain bit for bit equal for all subsequent times.

To ensure sufficient computational resolution and stability, the CFL condition and the condition on the degrees of freedom in two-dimensional turbulence given in ref. 27 were monitored for all computational runs. Let n by n be the grid size in physical space and Δt be the size of the time step. Let u and v be the x and y components of Eulerian velocity field. The CFL condition may be expressed as

$$\mathrm{CFL} = \frac{n\,\Delta t}{2L} \sup_{x \in \Omega} \{|u| + |v|\} \leqslant 1$$

and the condition on degrees of freedom may be expressed as

$$k_{\max} = \nu^{-1/2} \sup_{x \in \Omega} \left\{ \left|\frac{\partial u}{\partial x}\right|, \left|\frac{\partial v}{\partial x}\right|, \left|\frac{\partial u}{\partial y}\right|, \left|\frac{\partial v}{\partial y}\right| \right\}^{1/2} \leqslant \frac{n\pi}{L}.$$

For our final calculations we took $\nu = 0.0001$, $L = 2\pi$, $n = 169$, and $\Delta t = 0.04$. Thus, the Fourier transforms used to evaluate the nonlinear term were performed on a 256 by 256 spatial grid. Given these parameters, our final calculations obeyed

$$\mathrm{CFL} \leqslant 0.92 \qquad \text{and} \qquad k_{\max} \leqslant 82$$

and should, therefore, be well resolved.

Dependence of our numerical results on resolution was also studied directly. It should be noted that our experiment involves integrating a system with sensitive dependence on its initial conditions over a very long period of time. Thus, given different values for n and Δt otherwise identical calculations of u_1 will differ after long enough time. Even for identical values of n and Δt these calculations were observed to differ depending on the compiler and level of optimization used. The best we can hope for is that statistical properties including the rate of continuous data assimilation and number of determining modes remain unchanged. A number of preliminary tests with f, λ, and u_0 fixed were made to determine how our results depend on the exact values of n and Δt. Figure 9 illustrates the evolution of $\|u_1 - u_2\|$ for a set of resolution tests. These tests were conducted with the data assimilation parameter $\lambda = 26$ and the forcing function from Table I with $\lambda_f = 64$. It is clear that the rate of continuous data

Table III. Different Versions of Forcing Functions Supported on the Length Scales around $\lambda_f = 64$. The Rate α Was Measured for Continuous Data Assimilation on $N = 88$ Modes

Version	$\|f\|$	$\|f\|$	$\|f\|_*$	α
1	0.01928	0.0025	0.0003272	0.0105127
2	0.01905	0.0025	0.0003309	0.0102093
3	0.01921	0.0025	0.0003287	0.0099258
4	0.01923	0.0025	0.0003282	0.0104484
5	0.01919	0.0025	0.0003292	0.0112591

assimilation is independent of the resolution of the computation. Thus, we hope that our results are reasonably free from numerical artifacts.

Recall that the amplitudes of the Fourier components of f were chosen randomly with respect to a Gaussian distribution. Thus, our exact choice of f for each experiment was somewhat arbitrary. Table III explores for $\lambda_f = 64$ how the randomness in our choice of Fourier components for f affect the rate of continuous data assimilation. Notice that the V and V' norms of f vary by about one percent while the resulting rate of continuous data assimilation α varies by about three percent. We suppose all our results are within this margin for any reasonably probable choice of f.

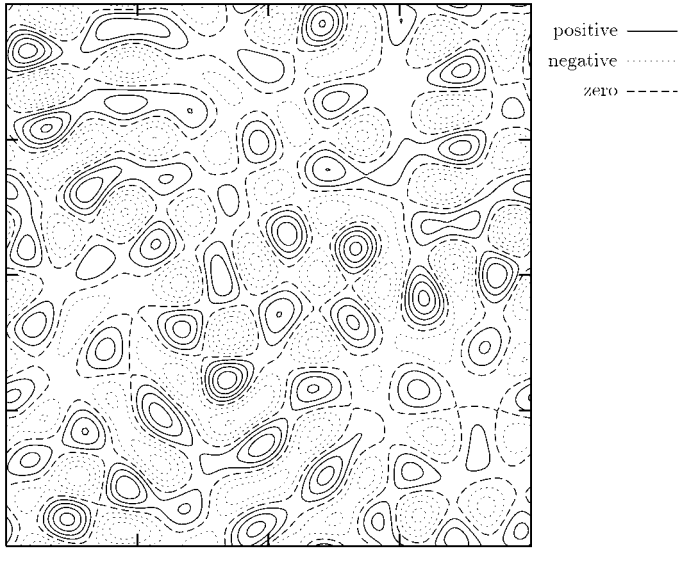

Fig. 8. Constant level curves of $g = \nabla \times f$ for $\lambda_f = 64$ illustrate the length scales present in the forcing.

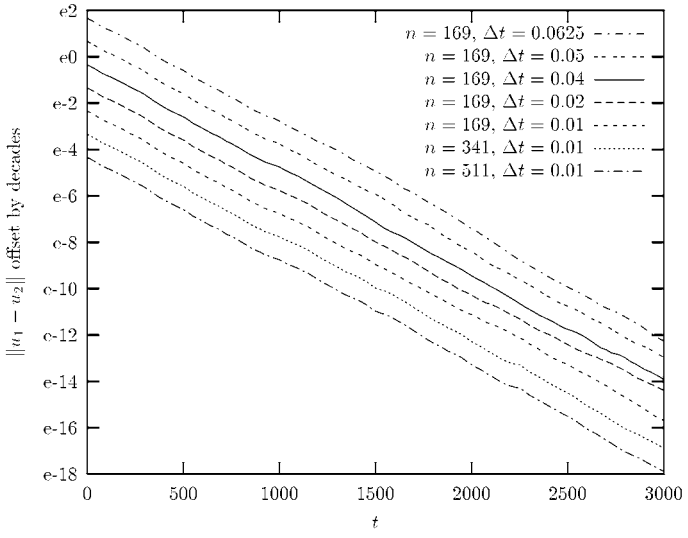

Fig. 9. The evolution of $\|u_1 - u_2\|$ for different values of n and Δt with $\lambda = 26$ and $\lambda_f = 64$ shows that the rate of continuous data assimilation is unrelated to the numerical resolution. The solid line represents the resolution of our final calculations. Other resolutions have been offset by decades for clarity.

An essential feature of a typical forcing function is that the spatial length scales are clearly exhibited while at the same time there are no additional symmetries. This feature is illustrated in Fig. 8 which gives the constant level curves of $\nabla \times f$ for the forcing function with $\lambda_f = 64$ from Table I. If, for example, f had additional periodic structure, then the initial condition u_0 and consequently u_1 and u_2 would also have this periodic structure. Thus, a rescaling such as in (1.8) would be possible. One could not expect the results from Table I to be relevant for such forcing functions.

One final remark is on our procedure for determining λ_c experimentally. Recall that λ_c was defined to be the smallest value of λ such that $\alpha \geqslant 0.0005$. This cutoff was chosen simply so that the evolution of $\|u_1 - u_2\|$ need not be computed for times much greater than $t = 25000$ to distinguish cases of convergence from nonconvergence. Therefore, it is possible that smaller values of λ would also show convergence. In such cases our λ_c still provides an upper bound on the number of determining modes, only perhaps not quite as sharp as possible.

6. CONCLUSIONS

We have studied a form of continuous data assimilation based on spectral modes for the two-dimensional incompressible Navier–Stokes

equations. Our work was inspired by the work of Browning *et al.*[2] and Kreiss and Yström,[33] who studied this form of continuous data assimilation in the case of zero body forcing. Our subject of interest has been how the spatial structure of a nonzero body forcing affects the rate of continuous data assimilation and the number of determining modes.

In our rigorous analysis we have shown that the equations governing continuous data assimilation on spectral modes are well posed. Moreover, we have found bounds on the number of spectral modes which guarantee that the approximations obtained by continuous data assimilation converge to the exact solution.

Our numerical simulations have shown that convergence actually occurs for a number of spectral modes much less than the upper bounds given by our rigorous results. Moreover, our simulations show an interesting maximum in the number of determining modes as the spatial structure of the forcing function is varied from large scales to small scales.

We finish by summarizing our explanation of this maximum. Forcing at large scales creates large scale motion within the fluid that control the small scale motion. In this case, only a few spectral modes are needed for continuous data assimilation to converge. Forcing at intermediate scales creates a turbulent flow but at the same time doesn't create the energetic large scale motion needed to control the small scales. In this case, continuous data assimilation requires more spectral modes to converge. Finally, forcing at very small scales creates no motion due to dissipation. In this case, no spectral modes are needed for continuous data assimilation to converge.

As a follow up we plan to study continuous data assimilation for random forces.

ACKNOWLEDGMENTS

This work was supported in part by the National Science Foundation under Grants DMS-9902360, DMS-9706964, DMS-9704632, and DMS-0204794. Partial support was also provided by the US Civilian Research and Development Foundation (CRDF) Cooperative Grants Program under Grant RM1-2343-MO-02. This work was completed while E.S.T. was the Stanislaw M. Ulam Visiting Scholar at the Center for Nonlinear Studies in the Los Alamos National Laboratory. We thank James Robinson and Sergei Chernyshenko for their useful comments on an earlier version of this paper.

REFERENCES

1. J. P. Aubin, Un théorème de compacité, *C. R. Acad. Sci. Paris Sér. I Math.* **256**: 5042–5044 (1963).

2. G. L. Browning, W. D. Henshaw, and H. O. Kreiss, A numerical investigation of the interaction between the large and small scales of the two-dimensional incompressible Navier–Stokes equations, UCLA CAM Technical Report 98–23, ftp://ftp.math.ucla.edu/pub/camreport/cam98-23[a-d].ps.gz, April 1998.
3. C. Canuto, M. Y. Hussaini, A. Quarteroni, and T. A. Zang, *Spectral Methods in Fluid Dynamics*, Springer Series in Computational Physics (Springer-Verlag, 1988).
4. C. Cao, M. A. Rammaha, and E. S. Titi, The Navier–Stokes equations on the rotating 2D sphere: Gevrey regularity and asymptotic degrees of freedom, *Z. Angew. Math. Phys.* **50**:341–360 (1999).
5. J. Charney, M. Halem, and R. Jastrow, Use of incomplete historical data to infer the present state of the atmosphere, *J. Atmos. Sci.* **26**:1160–1163 (1969).
6. B. Cockburn, D. A. Jones, and E. S. Titi, Determining degrees of freedom for nonlinear dissipative equations, *C. R. Acad. Sci. Paris Sér. I Math.* **321**:563–568 (1995).
7. B. Cockburn, D. A. Jones, and E. S. Titi, Estimating the number of asymptotic degrees of freedom for nonlinear dissipative systems, *Math. Comp.* **66**:1073–1087 (1997).
8. P. Constantin, C. R. Doering, and E. S. Titi, Rigorous estimates of small scales in turbulent flows, *J. Math. Phys.* **37**:6152–6156 (1996).
9. P. Constantin and C. Foias, *Navier–Stokes Equations*, Chicago Lectures in Mathematics (University of Chicago Press, Chicago, IL, 1988).
10. P. Constantin, C. Foias, and O. P. Manley, Effects of the forcing function spectrum on the energy spectrum in 2-D turbulence, *Phys. Fluids* **6**:427–429 (1994).
11. P. Constantin, C. Foias, and R. Temam, On the dimension of the attractors in two-dimensional turbulence, *Physica D* **30**:284–296 (1988).
12. R. Daley, *Atmospheric Data Analysis*, Cambridge Atmospheric and Space Science Series (Cambridge University Press, 1991).
13. A. Debussche and M. Marion, On the construction of families of approximate inertial manifolds, *J. Differential Equations* **100**:173–201 (1992).
14. C. Devulder and M. Marion, A class of numerical algorithms for large time integration: The nonlinear Galerkin methods, *SIAM J. Numer. Anal.* **29**:462–483 (1992).
15. C. Devulder, M. Marion, and E. S. Titi, On the rate of convergence on the nonlinear Galerkin methods, *Math. Comp.* **60**:495–514 (1993).
16. C. R. Doering and J. D. Gibbon, *Applied Analysis of the Navier–Stokes Equations*, Cambridge Texts in Applied Mathematics (Cambridge University Press, 1995).
17. T. Debios, F. Jauberteau, and R. Temam, The nonlinear Galerkin method for the two and three-dimensional Navier–Stokes equations. *Twelfth International Conference on Numerical Methods in Fluid Dynamics (Oxford, 1990)*, Lecture Notes in Phys., Vol. 371 (Springer, 1990), pp. 116–120.
18. C. Foias, M. S. Jolly, I. G. Kevrekidis, G. R. Sell, and E. S. Titi, On the computation of inertial manifolds, *Phys. Lett. A* **31**:433–436 (1988).
19. C. Foias, O. P. Manley, and R. Temam, Approximate inertial manifolds and effective viscosity in turbulent flows, *Phys. Fluids A* **3**:898–911 (1991).
20. C. Foias, O. P. Manley, and R. Temam, Iterated approximate inertial manifolds for Navier–Stokes equations in 2-D, *J. Math. Anal. Appl.* **178**:567–583 (1993).
21. C. Foias, O. P. Manley, R. Temam, and Y. Trève, Asymptotic analysis of the Navier–Stokes equations, *Physica D* **9**:157–188 (1983).
22. C. Foias and G. Prodi, Sur le comportement global des solutions non stationnaires des équations de Navier–Stokes en dimension two, *Rend. Sem. Mat. Univ. Padova* **39**:1–34 (1967).
23. C. Foias, G. R. Sell, and E. S. Titi, Exponential tracking and approximation of inertial manifolds for dissipative nonlinear equations, *J. Dynam. Differential Equations* **1**:199–244 (1989).

24. C. Foias and R. Temam, Determination of the solutions of the Navier–Stokes equations by a set of nodal values, *Math. Comput.* **43**:117–133 (1984).
25. C. Foias and R. Temam, *The connection between the Navier–Stokes equations, dynamical systems, and turbulence theory. Directions in partial differential equations* (Madison, WI, 1985), pp. 55–73, Publ. Math. Res. Center Univ. Wisconsin, Vol. 54 (Academic Press, Boston, MA, 1987).
26. M. Frigo and S. G. Johnson, The fastest fourier transform in the west, MIT Technical Report, MIT-LCS-TR-728, http://www.fftw.org/ (1997).
27. W. D. Henshaw, H. O. Kreiss, and L. G. Reyna, On the smallest scale for the incompressible Navier–Stokes equations, *Theor. Comp. Fluid Dynam.***1**:65–95 (1989).
28. M. J. Holst and E. S. Titi, Determining projections and functionals for weak solutions of the Navier–Stokes equations, *Recent Developments in Optimization Theory and Nonlinear Analysis* (Jerusalem, 1995), Contemp. Math., Vol. 204 (Amer. Math. Soc., Providence, RI, 1997), 125–138.
29. M. S. Jolly, Bifurcation computations on an approximate inertial manifold for the 2D Navier–Stokes equations, *Physica D* **63**:8–20 (1993).
30. M. S. Jolly, I. G. Kevrekidis, and E. S. Titi, Approximate inertial manifolds for the Kuramoto–Sivashinsky equation: analysis and computations, *Physica D* **44**:38–60 (1990).
31. D. A. Jones and E. S. Titi, On the number of determining nodes for the 2D Navier–Stokes equations, *J. Math. Anal. Appl.* **168**:72–88 (1992).
32. D. A. Jones and E. S. Titi, Upper bounds on the number of determining modes, nodes, and volume elements for the Navier–Stokes equations, *Indiana Univ. Math. J.* **42**:875–887 (1993).
33. H. O. Kreiss and J. Yström, Numerical experiments on the interaction between large and small-scale motion of incompressible turbulent flows, *J. Fluid Mech.*, to appear.
34. O. A. Ladyzhenskaya, *The Mathematical Theory of Viscous Incompressible Flow*, 2nd English Ed., Translated from the Russian by Richard A. Silverman and John Chu, Mathematics and Its Applications, Vol. 2 (Gordon & Breach, Science Publishers, New York, 1969).
35. O. A. Ladyzhenskaya, On the dynamical system generated by the Navier–Stokes equations, *J. Soviet Math.* **3**:458–479 (1975).
36. J. L. Lions and E. Magenes, *Nonhomogeneous Boundary Value Problems and Applications* (Springer, Berlin, 1972).
37. C. Marchioro, An example of absence of turbulence for any Reynolds number, *Comm. Math. Phys.* **105**:99–106 (1986).
38. N. Platt, L. Sirovich, and N. Fitzmaurice, An investigation of chaotic Kolmogorov flows, *Phys. Fluids A* **3**:681–696 (1991).
39. J. C. Robinson, *Infinite-Dimensional Dynamical Systems: An Introduction to Dissipative Parabolic PDEs and the Theory of Global Attractors*, Cambridge Texts in Applied Mathematics (Cambridge Unniversity Press, 2001).
40. R. Temam, *Navier–Stokes Equations: Theory and Numerical Analysis*, revised edition (AMS Chelsea Publishing, 1984).
41. R. Temam, *Navier–Stokes Equations and Nonlinear Functional Analysis*, 2nd ed., CBMS-NSF Regional Conference Series in Applied Mathematics, Vol. 66 (SIAM, 1995).
42. E. S. Titi, On a criterion for locating stable stationary solutions to the Navier–Stokes equations, *Nonlinear Anal.* **11**:1085–1102 (1987).
43. Y. M. Trève and O. P. Manley, Minimum number of modes in approximate solutions of equations of hydrodynamics, *Phys. Lett. A* **82**:88 (1981).